Environment CANADA Environnement
10209261 VOL ISS 66 850700
EXC # 001
TD 171.5.C3 R46
REPORT EE

OOFF

DETERMINATION OF OCEANOGRAPHIC FACTORS ASSOCIATED WITH THE SUBSURFACE MOVEMENT OF OIL

EE-66

DETERMINATION OF OCEANOGRAPHIC FACTORS ASSOCIATED WITH THE SUBSURFACE MOVEMENT OF OIL

by

B.A. Juszko
Atlantic Oceanics Co. Ltd.
Dartmouth, Nova Scotia

This report has not undergone detailed technical review by the Environmental Protection Service and the content does not necessarily reflect the views and policies of Environment Canada. Mention of trade names or commercial products does not constitute endorsement for use.

This report is the result of a contract let under PERD funding in the Atlantic Region. This unedited version is undergoing a limited distribution to transfer the results to people working in related research. This distribution is not intended to signify publication and, if the report is referenced, the author should cite it as an unpublished report of the Branch indicated below.

Any comments concerning its content should be directed to:

Technical Services Branch
Environmental Protection Service
Environment Canada
Ottawa, Ontario
K1A 1C8

Marine Environment Protection Branch
EPS Atlantic Region
Environment Canada
45 Alderney Drive
Dartmouth, Nova Scotia
B2Y 2N6

EE-66

July, 1985

TABLE OF CONTENTS

		Page
TABLE OF CONTENTS		i
LIST OF FIGURES		ii
LIST OF TABLES		iii
LIST OF SYMBOLS USED		iv
EXECUTIVE SUMMARY		vi
1.	INTRODUCTION	1
2.	SPATIAL AND TEMPORAL SCALES	2
3.	MACROSCALE FEATURES	6
	3.1 Mean Coastal Circulation	7
	3.1.1 Atlantic Coast	7
	3.1.2 Southeastern Beaufort Sea	12
	3.2 Mean Seasonal Density Distribution	15
	3.2.1 Atlantic Coast	15
	3.2.2 Southeastern Beaufort Sea	26
	3.3 Topographically Related Features	28
	3.4 Macroscale Waves and Eddies	31
4.	MESOSCALE FEATURES	32
	4.1 Mesoscale Waves	32
	4.2 Frontal Features - Dynamics and Cross-frontal Exchange	35
	4.3 Longitudinal Mixing	39
	4.4 Langmuir Circulation	41
5.	MICROSCALE FEATURES	43
	5.1 Vertical Mixing	43
	5.2 Behaviour of Suspensions	51
6.	IMPLICATIONS FOR THE BEHAVIOUR OF OIL SPILLS	52
7.	CONCLUSIONS AND SUGGESTIONS FOR FUTURE WORK	66
8.	REFERENCES	68

LIST OF FIGURES

Figure No.			Page
2.1		Spatial and Temporal Scales	3
3.1		Reference Chart for the Atlantic Coast	8
3.2		Reference Chart for the Southeastern Beaufort Sea	13
3.3	(a)	Representative vertical density profiles on the Labrador Shelf (from Juszko et al., 1983)	16
3.3	(b)	Representative vertical density profiles on Newfoundland's Grand Banks (from Juszko et al., 1983)	17
3.3	(c)	Representative vertical density profiles for the Gulf of St. Lawrence (from Juszko et al., 1983)	18
3.3	(d)	Representative vertical density profiles for the Scotian Shelf and Gulf of Maine (from Juszko et al., 1983)	19
3.4		Cross-shelf density distribution on the Labrador Shelf (Summer) (from Juszko et al., 1983)	20
3.5	(a)	Cross-shelf property distribution at the Halifax Section (Summer - from de La Ronde (1972))	23
3.5	(b)	Cross-shelf property distribution at the Halifax Section (Winter - from de La Ronde (1972))	24
3.6		Contoured surface densities in the Bay of Fundy and Gulf of Maine - Summer (from Juszko et al., 1983)	25

LIST OF TABLES

Table No.		Page
3.1	Summary Current Statistics	9
3.2	Summary of Temperature - Salinity - Density Properties	21

LIST OF SYMBOLS USED

- B - buoyancy flux
- c - scalar concentration
- Co - Cox number
- ^oC - Degress Centigrade
- C_d - drag coefficient
- C_w - wave phase speed
- d - droplet diameter
- D_c - molecular diffusivity of a scalar, c.
- e_v - viscous dissipation inside on turbulent patch
- E_k - Ekman number
- f - Coriolis parameter
- g - acceleration due to gravity
- H,h - water depth
- H_E - vertical dimension of a turbulent patch
- k - wavenumber
- k_g - cut off wavenumber above which wave breaking occurs
- k_{vK} - von Karman's constant
- K_h - horizontal eddy diffusivity
- K_v - vertical eddy diffusivity
- L_l - tidal excursion
- L_B - Batchelor scale
- L_E - Ekman depth
- L_K - Kolmogorov scale
- L_M - mean turbulent eddy diameter
- L_R - Osmidov or buoyancy scale
- M - momentum
- N - Brunt-Vaisala frequency
- R_e - Estuarine Richardson Number
- R_i - Richardson Number
- R_f - Flux Richardson Number
- T - period of an oscillating current
- T_c - time scale for mixing over water depth

T_g - wave period associated with k_g

T_L - Lagrangian time scale

T_m - time scale for movement around an eddy with diameter, L_m

T_T - time scale for lifetime of a turbulent patch

u - horizontal current velocity

$u*$ - friction velocity

U_l - tidal velocity

U_T - RMS Eulerian eddy velocity

U_{10} - wind speed at 10 meters height

v_d - RMS velocity difference over a distance d

w - vertical current velocity

w_T - terminal velocity

W - wind speed

$W*$ - turbulent surface friction velocity (square root of shear stress) related to wind mixing

W_B - buoyancy velocity

o/oo - parts per thousand (salinity)

β (beta) - Beta parameter

γ (gamma) - rate of strain of turbulence

γ_o - rate of strain of turbulence at time of fossiliation

γ_s - non-dimensional mean bottom slope

ϵ (epsilon) - energy flux (dissipatin rate of turbulent kinetic energy)

ζ (zeta) - ratio of tidal/residual RMS velocity

θ (theta) - angle

λ (lambda) - ratio of tidal/residual light scale

ν (nu) - eddy viscosity

ρ (rho) - density

σ_t (sigma) - sigma - t (density x 10^3 - 1000)

τ (tau) - surface tension

Φ (phi) - volume fraction of particles in a suspension

ω (omega) - frequency

EXECUTIVE SUMMARY

A literature review was conducted in order to examine the various physical oceanographic features which could contribute to the subsurface movement of oil. Observations in five geographic areas along Canada's coasts (Grand Banks of Newfoundland, Gulf of St. Lawrence, Scotian Shelf, Bay of Fundy - Gulf of Maine and the Canadian Beaufort Sea) were used to illustrate these features. The various processes were described in terms of the spatial and temporal scales governing their behaviour. They were divided into three categories (macroscale, mesoscale and microscale) in order to illustrate both the principles behind parameterization of processes and the various levels of resolution required in modelling them. The macroscale features discussed included the general circulation patterns, seasonal water density distributions, topographically related features (fronts and frontal circulation, upwelling and rectified flows) and macroscale waves and eddies. The latter were illustrated by examination of topographic Rossby waves at the Scotian Shelf/Slope boundary and Gulf Stream Rings. The dynamics governing the formation and propagation of internal waves, the structure of fronts, longitudinal mixing and Langmuir circulation were discussed under mesoscale features. This included observations near melting icebergs. Turbulence, and its associated length and time scales, was examined as the primary microscale feature governing the eventual dispersion of subsurface oil. Particular reference was made to the surface mixed layer and the influence of breaking waves contributing to oil dispersal. A cursory overview of microhydrodynamics is included.

The various features were then related to oil spill behaviour through the examination of an idealistic four-dimensional model. The major conclusions and recommendations were for a better integration of physical oceanographic processes and oil chemistry in both laboratory experiments and model designs. These should include the possible synergistic behaviour between processes, the influence of other parameters in the water column (ex. suspended sediment, air bubbles) on the oil and potential modifying effects of oil on the physical oceanography.

1. INTRODUCTION

Although all types of oil have initial densities less than that of water, there have been various historical examples of oil spills where the oil, or oil fraction, has sunk below the water surface impeding clean-up procedures. At other times, the sinking of oil had been instigated through the use of emulsifying agents. Once below the surface, the behaviour of the oil will depend on both the physical and chemical characteristics of the oil, or oil fraction, and the various oceanographic features it encounters.

This report examines the subsurface movement of oil by primarily discussing the spatial and temporal scales of both permanent and sporadic oceanographic features encountered in Canadian Atlantic waters and in the Canadian Beaufort Sea. As examination of the behaviour of oil is currently being done via the use of analytical and numerical models, it is the scales chosen which will determine which oceanographic processes can be parameterized and which must be detailed. The method of handling the process requires understanding of the physics governing it. Selected Atlantic and Beaufort Sea sites will illustrate the use of oceanographic scales in light of model requirements. Conclusions and suggestions are then given on the requirements of oil spill modelling and future areas of research.

2. SPATIAL AND TEMPORAL SCALES

The movement of oil, or an equivalent water parcel, will depend on both the advective, or "organized", and the dispersive, or "disorganized", characteristics of the velocity field. The various oceanographic features giving rise to this velocity field are most easily examined through consideration of their spatial and temporal scales. The classification of oceanographic features in terms of macro-, meso- and microscale ranges will be based on fixed physical characteristics. However, the separation into "organized" and "disorganized" motion is somewhat subjective and many oceanographic features can be treated as one or the other, depending on the spatial and temporal scales chosen as reference. This approach often proves convenient for modelling a given process as one can often superimpose larger scale motion as a mean behaviour and parameterize the much smaller scales (i.e., treat the interactions at smaller scales like a "black box") without examining the specific interactions at these scales. In some cases, motions at scales beyond the range of interest can be ignored completely. An understanding of the oceanographic features included in all three scale ranges is also important for real-time applications such as oil spill clean-up operations. These require a knowledge of the existing conditions, not only in a mean sense, but also in the perturbation about this mean. In terms of macroscale features, this includes ascertaining the local seasonal characteristics of the water column, ice cover and current velocities, the existing positions of fronts and current jets and the presence of any unusual though influential features (for ex: Gulf Stream Rings). As the clean-up operation may last days to weeks, variability on these time scales would have to be understood such as storm forcing, frontal meanders, etc. Daily procedures would require knowledge of tides and tidal fronts. Superimposed are the smaller scale processes acting to disperse or concentrate the spill locally, influencing both the equipment used for recovery and the level of effort required.

The spatial and temporal scales of variability will be treated, by analogy, to those of organized wave motion according to the ranges set out by Nihoul (1980) and the vertical wavenumber scale of Holloway (1983). These are superimposed on a given "mean" behaviour chosen as some larger spatial scale. Figure 2.1 schematically illustrates these scales in relation to observed oceanographic features. Solid lines represent the wavenumber/frequency range while dashed lines correspond to length (meters) and time (seconds). Generally, length and time (or wavenumber and frequency) behave similarly both decreasing (or increasing) as one moves to the right

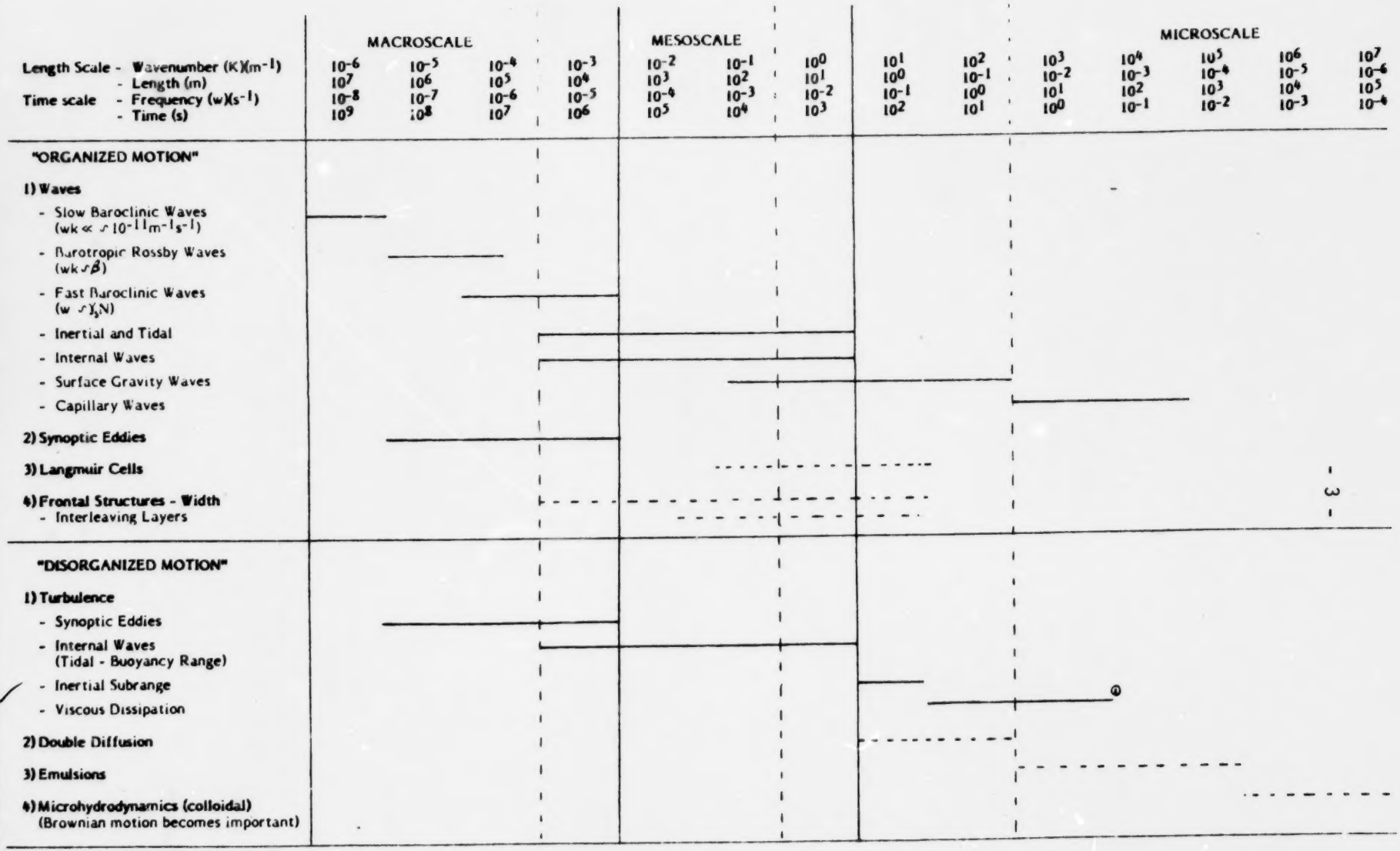
MACROSCALE
MESOSCALE
MICROSCALE
Length Scale - Wavenumber (K)(m⁻¹)
- Length (m)
Time scale - Frequency (w)(s⁻¹)
- Time (s)
10⁻⁶ 10⁻⁵ 10⁻⁴ 10⁻³ 10⁻² 10⁻¹ 10⁰ 10¹ 10² 10³ 10⁴ 10⁵ 10⁶ 10⁷
10⁷ 10⁶ 10⁵ 10⁴ 10³ 10² 10¹ 10⁰ 10⁻¹ 10⁻² 10⁻³ 10⁻⁴ 10⁻⁵ 10⁻⁶
10⁻⁸ 10⁻⁷ 10⁻⁶ 10⁻⁵ 10⁻⁴ 10⁻³ 10⁻² 10⁻¹ 10⁰ 10¹ 10² 10³ 10⁴ 10⁵
10⁹ 10⁸ 10⁷ 10⁶ 10⁵ 10⁴ 10³ 10² 10¹ 10⁰ 10⁻¹ 10⁻² 10⁻³ 10⁻⁴
"ORGANIZED MOTION"
1) Waves
- Slow Baroclinic Waves (wk ≪ ~10⁻¹¹m⁻¹s⁻¹)
- Barotropic Rossby Waves (wk~β)
- Fast Baroclinic Waves (w ~ Y,N)
- Inertial and Tidal
- Internal Waves
- Surface Gravity Waves
- Capillary Waves
2) Synoptic Eddies
3) Langmuir Cells
4) Frontal Structures - Width
- Interleaving Layers
ω
"DISORGANIZED MOTION"
1) Turbulence
- Synoptic Eddies
- Internal Waves (Tidal - Buoyancy Range)
- Inertial Subrange
- Viscous Dissipation
a
2) Double Diffusion
3) Emulsions
4) Microhydrodynamics (colloidal) (Brownian motion becomes important)

Note (1) Time scales in the dissipation range are no longer decreasing monotonically.

Figure 2.1 Spatial and Temporal Scales

on Figure 2.1. However, in the viscous dissipation scales of turbulence, time scales again increase due to the slower energy transfer by molecular processes (i.e., viscous) than by eddy momentum exchange (see Tennekes and Lumley, 1972).

The length scales of wave motion in the macroscale range, wavenumbers of 10^{-6} to 10^{-3} m^{-1}, are governed by the spatial variation of the Coriolis parameter given by $\beta \sim 10^{-11}$ m^{-1} s^{-1} (Nihoul, 1980). Variation of the Earth's rotation rate is the chief restoring force at this scale. These include very slow baroclinic waves ($\omega k \ll \beta$, ω = frequency, k = wavenumber), barotropic Rossby waves ($\omega k \sim \beta$) and fast baroclinic waves ($\omega \sim \gamma_s$ N), γ_s = non-dimensional mean bottom slope, N = Brunt-Vaisala frequency) (see Nihoul, 1980). Oceanographic features in this range include the very large scale (hemispherical) current gyre systems, the smaller scale synoptic eddies (ex., Gulf Stream Rings) and current and front meanders. The time scales range from years down to weeks incorporating seasonal changes due to changes in weather, ice cover, fresh water runoff, etc., and non-synoptic forcing (i.e., non meteorological). There is some overlap with the mesoscale range for synoptic flow forcing (i.e., meteorological 2 - 10 day periods).

The mesoscale is delineated by motions having gravity as the chief restoring force. The rotation of the earth is considered to be constant and to act only to modify the effect of gravity. Motion at these scales may have a surface (barotropic) or internal (baroclinic) expression. The pass-band for internal waves is characterized by the inertial frequency (lower limit) and the Brunt-Vaisala frequency (upper limit). Oceanographic features in this scale include semi-diurnal and diurnal surface and internal tides, Kelvin waves, Poincare waves and surface (upper end) and internal gravity waves. The length scales include motions covering fractions of the ocean surface (in the case of tides) to meters with corresponding time scales of several days to several seconds.

The microscale motions are no longer affected by buoyancy, that is, they have frequencies larger than the maximum Brunt-Vaisala frequency (O (10^{-2}) sec). Surface capillary waves, whose restoring force is surface tension, can be considered as a microscale feature.

"Disorganized motion", in this application, includes all mixing processes as well as the very small scale particle interactions occurring in suspensions and colloids. It is this "disorganized motion" which will eventually lead to the dispersal of an oil spill and it is the length scales of the motion which will determine the

character of the dispersed oil. Mixing by means of eddies is generally termed "turbulence" and can be treated in a spectral sense as an energy cascade from small to large wavenumbers. A spectral treatment is useful due to direct links with spectra of turbulence producing physical features, such as breaking internal or surface gravity waves, size spectrum of bottom topographic features, etc. The turbulence spectra can also be related by analogy to spectra of turbulence "signatures", for example, particle size spectrum of air bubbles (or oil droplets) in the surface mixed layer and microstructure measurements. The level of turbulence in the surface mixed layer will impose limits on oil droplet formation. As with "organized motion", mixing by wavenumbers beyond the range of interest may be parameterized or ignored, and in most applications, horizontal and vertical mixing is parameterized using an eddy viscosity (for momentum) or eddy diffusivity (for a scalar). The nature of the turbulence at wavenumbers of interest, is based on the inter-relationship between various properties of the flow: ν, eddy viscosity; ϵ, energy flux or dissipation rate; N, Brunt-Vaisala frequency; and, for a scalar, D_c, molecular diffusivity. At all scales, turbulence receives its energy from the mean flow. Large eddies then act to strain smaller ones, thereby increasing the vorticity of these smaller eddies with a consequent increase in their energy. In the process, the larger eddies lose energy. At very small scales, an equilibrium range exists such that the eddies exhibit local isotropy and the total amount of energy transfer is equal to ϵ. In this viscous dissipation range, the energy is scaled as a function of the product of the wavenumber and the Kolmogorov miscroscale L_k ($L_k = (\nu/\epsilon)^{1/4}$). The lower limit of this range is of the order $L_k = 1$ and the upper limit is set by the smallest time scale, $(\nu/\epsilon)^{1/2}$. If the Reynolds number is sufficiently large, an inertial subrange exists within which no energy is added by the mean flow and no energy is taken out by viscous dissipation. The energy flux here is equal to ϵ and the energy at each wavenumber is proportional to $k^{-5/3}$. Scales of contaminant fluctuations range from the scale of energy containing eddies to a smallest scale that depends on the ratio of diffusivities (eddy and molecular). Because of the different magnitudes of the two diffusivities, various subranges can exist in both the inertial and viscous dissipation regions. These concepts are discussed further in Section 5 and for a complete analysis, see Tennekes and Lumley (1972).

In the following sections, concepts introduced here will be examined more fully with reference to the existing oceanographic features in the geographic areas of interest. Within each section, discussion will progress from larger to smaller scales.

3. MACROSCALE FEATURES

As mentioned in the previous section, an understanding of the macroscale features of coastal waters is required for both modelling of oil spills and in real-time operations. Three levels of model sophistication can be used. The lowest level consists of order of magnitude estimates of spill volume and volume transport over a set time period. This approach is useful for delineating the potential areal coverage of a spill of initial set size, coastal impact areas, percentages of dispersed oil, etc. It can point to regions where more sophisticated approaches are required. The second level treats macroscale features of the circulation and water column as constant background conditions varying much more slowly than the time scale of interest, and upon which smaller scale processes are examined in detail. The background constants can be annual or seasonal means or observed extreme conditions. For this approach, field observations may be sufficient, however, understanding of the physics influencing the macroscale features is still required when applying model results to real situations. The third level of modelling determines the circulation pattern explicitly using a numerical scheme by which an initially stationary fluid is forced into motion. The model equations are based on theoretical concepts and field observations are now used for calibration. Such a model is often used as a diagnostic tool to estimate the sensitivity of different forcing mechanisms. Because of their large size, these models are usually limited in areal coverage. Thus their usefulness lies in specific site applications or in specifying the initial background conditons within a survey grid for use by a lower level model. For real-time operations, qualitative understanding of spatial and temporal flow variability is required to allow for on site flexibility in response to the observed situation.

The following sections 3.1 and 3.2 describe observed, or inferred, circulation patterns and water density profiles for Canada's Atlantic Coast and the Canadian Beaufort Sea. When available, ranges in flow estimates are given. The flow forcing and density controlling processes are detailed. Section 3.3 discusses topographically related features and Section 3.4 overviews macroscale waves both of which result in spatial variability in the mean circulation.

3.1 Mean Coastal Circulation

3.1.1 Atlantic Coast

Figure 3.1 contains a chart of the southern Atlantic coast of Canada upon which is superimposed the summer mean circulation patterns. This pattern would reflect, in a broad sense, the transport in surface spilled or dispersed oil at a given location. In the discussion of mean circulation, it must be kept in mind 1) that the characteristics of the current will vary on time scales ranging from seasonal down to a few days in response to changes in forcing; 2) that superimposed on the residual current will be tidal and inertial oscillations; and 3) that the currents will be composed of both barotropic and baroclinic components, particularly important when considering subsurface movement of oil. Table 3.1 summarizes speed and transport measurements for the discussed flows. The sources of data are varied, different methods used each having their own limitations, and as such the values listed should not be taken as absolute.

The Labrador Current flows southward from Hudson Strait along the coast of Labrador and Newfoundland. It is composed of two branches. The inshore branch of the Labrador Current consists of Baffin Land Current water (not shown), which flowing through Davis Strait gets mixed with cold, low salinity water exiting Hudson Strait. The offshore branch follows the shelf break and is composed of a mixture of Labrador Sea water and West Greenland current water.

At the Strait of Belle Isle, some water from the inshore branch can travel through the Strait to enter the Northeast Gulf of St. Lawrence (see Huntsman et al., 1954, Farquarson and Bailey, 1966) while outflow from the Gulf may also occur contributing to waters on the East coast of Newfoundland. This strait is subject to very large tidal and mean currents, particularly in the narrows, with maximum tidal and residual currents both on the order of 2 m/s (e.g. Farquarson and Bailey, (1966) 1980 CSS Dawson cruise data). The residual flow is thought to be a response to sea level differences between the Gulf of St. Lawrence and the Labrador Shelf set-up by geostrophic winds parallel to Esquiman Channel (affecting the Gulf) or parallel to the East Coast of Labrador (affecting Labrador Shelf) (Garrett and Petrie, 1981; Garrett and Toulany, 1981, 1982). Hence variability of the residual flow in the strait is on meteorological time scales and the flow can change from complete inflow, variable levels of inflow along the Labrador side and outflow along Newfoundland, or complete outflow. In each situation the vertical current profile would vary.

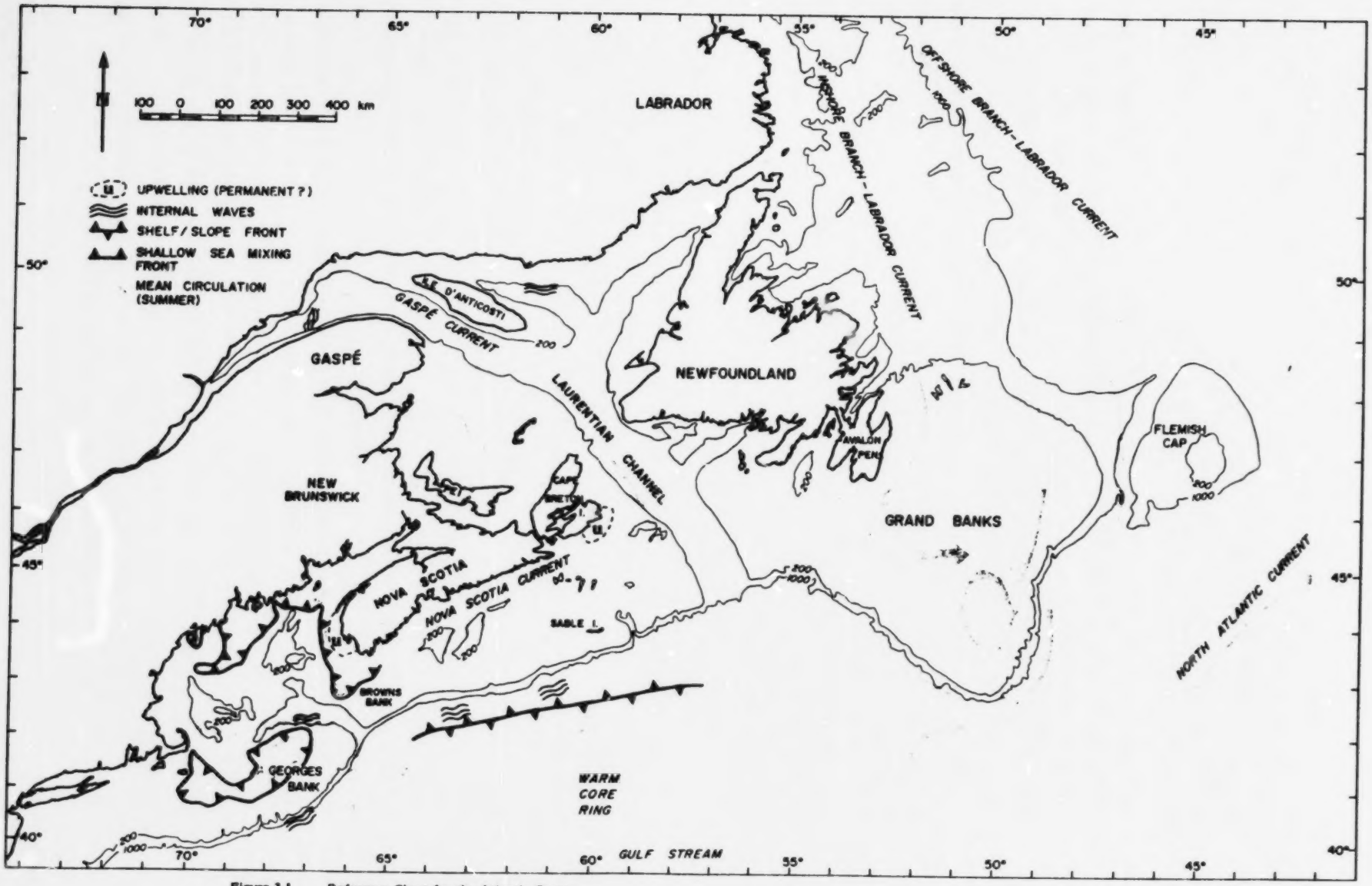

Figure 3.1 Reference Chart for the Atlantic Coast

Table 3.1

Summary Current Statistics

Current Description	Residual Speeds m/s	Estimated Transports 10^6 m^3/s	Reference
Labrador Current			
Inshore Branch			
North of Strait of Belle Isle	- 0.2	06 - 1.5 -	Matthews (1976) Petrie and Anderson (1983)
Through Avalon Channel	.05 - .2	0.6	Petrie and Anderson (1983)
Offshore Branch			
North of Strait of Belle Isle	-	3.6 - 4.2	Matthews (1976)
Off Bonavista Bay	.3	-	Petrie and Anderson (1983)
Edge of Grand Banks (east)	.2 - .6	4.1	Petrie and Andeson (1983)
	-	3.3	McLellan (1957)
Edge of Grand Banks (west)	.15 - .25	-	Petrie and Anderson (1983)
On Top of Bank	.02 - .1		Petrie and Anderson (1983)
Strait of Belle Isle			
Surface	.03 - 1.7	.14	Juszko (1981)
Subsurface	.04 - .5	(net into Gulf)	
Cabot Strait			
Outflow	.2 - .5 (August)	.43 - .84	El-Sabh (1975)
Inflow	.14 (Max.: November)	.41 - .74	Trites (1971) Cootes and Yeats (1979)
St. Lawrence River	-	.014 - .031 (February)(May)	El-Sabh (1975)
Gaspe Current	.35 - 1.1 (Max.: May - June)	-	El-Sabh (1975) Benoit et al (1985)
Nova Scotia Current	.01 - .1 (July)(January)	.15 1.0	McLellan (1957) Drinkwater et al., (1979) Sutcliffe et al (1976)
Eastward Slope Current	.1 - .20		Horne (1978), Smith and Petrie (1982)
Westward Subsurface Slope Current	~ .02		Smith and Petrie (1982)
Into Gulf of Maine	.04 - .1	.14 (max. .35) .17 .25	Smith (1983) Hopkins & Garfield (1979) Vermersh et al.(1979)
Circulation on Browns Bank	.05 - .15		Smith (1983)
Circulation on Georges Bank			
Surface	.15 - .30		Butman et al. (1982)
Subsurface (75 m)	.05		Marsden (1985)
In Minas Channel	≤0.5		Greenberg (1983)
Gulf Stream Surface	up to 2.5	40 - 90	Stommel (1965)

Both branches of the Labrador current continue to travel down the East Coast of Newfoundland. At approximately 48°N the current impinges on the northern edge of the Grand Banks. A good review of the circulation on the Newfoundland continental shelf is provided by Petrie and Anderson (1983) and the following is extracted from their findings. The offshore branch flows around the edge of the bank in response to topographic steering effects. Some of the flow is directed around Flemish Cap. At the Tail of the Grand Banks, part of the flow turns eastward to join the North Atlantic Current while the remainder continues along the edge and eventually travels through Cabot Strait into the Gulf of St. Lawrence where it forms the Deep Gulf water, part of the estuarine circulation system. This pattern can be observed by following the freshwater pulse generated in the Arctic in spring. Its signature can be seen in hydrographic data from the eastern edge of the Grand Banks in August -September and in Cabot Strait by November. The inshore branch flows westward around the Avalon Penisula. As much as 80% of the water will be diverted offshore to join the slope water current while the rest may enter the Gulf of St. Lawrence through Cabot Strait and progress northward along the west coast of Newfoundland. Flow on top of the Bank is weak and subject to local wind forcing with strong inertial motions at periods of 16 hours. In the winter, the water column is mixed to the bottom and will respond, as a whole, to the wind. Stratification in the summer can uncouple the surface and bottom layers, resulting in depth dependent motion.

A general review of the physical and chemical characteristics of the Gulf of St. Lawrence can be found in Trites and Walton (1975) with estimates of current speed and volume transports in El-Sabh (1975). The Gulf of St. Lawrence is characterized by its estuarine nature, by the presence of two major channels, the Laurentian Trough and Esquiman Channel, and by two accesses to the open ocean, Cabot Strait and the Strait of Belle Isle. The Gulf of St. Lawrence can be considered as composed of five regions each having distinct physical characteristics. The Upper Estuary region extends from the upper reaches of the St. Lawrence River to the tip of the Gaspe Peninsula. A salinity signature can be observed as far upstream as Quebec City. The estuary is composed of a "well-mixed" type at the head, "moderately-mixed" until approximately the Saguenay River, and stratified in the lower part (El-Sabh, 1984). This is related to the relative depths and extension of the Laurentian Trough. In the lower estuary, a separation of flows occurs as the channel widens, with a concentration of outflow along the Gaspe shore and at the surface and inflow below and to the North along the Anticosti side of the Gaspe Passage. Also

observed is a series of alternating eddies accompanied by transverse currents in the lower part (El-Sabh, 1984). A permanent cyclonic gyre exists west of Anticosti Island. Much of the outflow is concentrated in the Gaspe Current which rounds the Gaspe Peninsula and then broadens over the Magdalen Shallows. The Magdalen shallows are characterized by reduced water depths with a generally southward circulation (.1 - .2 m/sec) which converges and intensifies towards Cabot Strait. The Central Gulf is composed of the two major channels and the waters here have a distinct three layer structure in the summer (see Section 3.2). The surface circulation is composed partly by the outflow from the Gaspe passage. Joined by the inflow at Cabot Strait of inshore Labrador Current water, much of the surface waters head up Esquiman Channel towards the Strait of Belle Isle. A gyre over Mecatina Bank results in a return flow along the north shore and above Anticosti. The flow through the Strait of Belle Isle is meteorologically driven, with possibly greater inflow of Labrador water in the winter (Garrett and Petrie, 1981; Garrett and Toulany, 1981). Flow through Cabot Strait, partially estuarine driven, does not show the same variability, with a generally constant outflow along the Cape Breton Island shore at times extending across the Strait at the surface, with inflow below and along the Newfoundland coast. The strongest outflow occurs in August related to the peak in river disharge with the strongest inflow in November associated with the freshwater pulse carried by the Labrador current.

Water exiting through Cabot Strait forms part of a generally westward drift along the Nova Scotian Shelf, called the Nova Scotian Current by Bigelow (1927). The shelf water is actually a mixture of Gulf of St. Lawrence water and Slope water (McLellan, 1954). Over the continental slope, two water types can be found. The surface waters are warm and saline, with a generally eastward flow, while below 200 m there exists a mixture of Labrador and North Atlantic central water which drifts westward (Gatien, 1976). Further offshore lies the Gulf Stream, forming a variable boundary between the slope water and the Sargasso Sea. A shelf-slope boundary also exists, showing strong contrasts in temperature and salinity with little density change (Horne, 1978). The flow at the boundary is influenced by various processes and will be discussed further in Section 3.3. The Nova Scotian Current rounds Cape Sable and forms a major input to the Gulf of Maine - Bay of Fundy circulation. The dominant feature of this region is the large tidal amplitudes and much of the residual circulation can be explained through the non-linear interactions of the tides and bathymetry (tidal rectification) or by density driven flows between areas of different stratification caused by tidal mixing. The general circulation here

was first described by Bigelow (1927). The Gulf of Maine consists primarily of a large cyclonic gyre over the central area with inflow up the Bay of Fundy along Nova Scotia, return flow along the New Brunswick shore, and a strong clockwise circulation around Georges Bank, resulting in waters exiting through the Northeast Channel. There is some seasonal variation in the strength of these gyres. The barotropic model of Greenberg (1983) and the depth averaged baroclinic model of Isaji and Spaulding (1984) reproduce many of the features of this residual circulation and do prove useful for both theoretical and practical applications.

3.1.2 Southeastern Beaufort Sea

Figure 3.2 contains a chart of the southeastern Beaufort Sea illustrating the major oceanographic features.

The general circulation (summer) consists of a large anti-cyclonic gyre over the Canadian Basin which is intensified over the continental slope to form a jet of 0.1 m/s parallel to the local bathymetric contours (Melling, 1983). On top of the shelf, the mean currents flow towards the Northeast with super-imposed variability primarily due to inertial oscillations. These are highly baroclinic, due to stratification supplied by surface heating and Mackenzie River input (Fissel, 1981). At this latitude, the period of inertial oscillations overlaps with the range of semi-diurnal tidal components and it is often difficult to separate the two contributions. An examination of direct current measurements (Fissel, 1981; Melling, 1983) showed mean bottom currents toward the Northeast of .03 - .08 m/s. From hydrographic data over the Northeast Mackenzie shelf, Melling (1983) calculated a mean eastward flow of .05 - .06 m/s near the seafloor, weaker easterly flow at mid-depth (.03 - .04 m/s) and less than .01 m/s at the surface due to the observed baroclinic shear. By observations of ice floes, Khandekar (1980) estimated a .04 m/s inertial oscillation at the surface. Mean and maximum surface currents of .19 m/s and .70 m/s, respectively, have been measured directly (Fissel, 1981). The position of the Mackenzie River plume, in the summer, depends on both wind direction and the position of the ice edge. The eastward flow in the plume reflects both buoyancy and Coriolis force influence. The eastward flow near bottom is suggested by Melling (1983) to result from a haline circulation which is forced by water freezing. The denser water left behind would tend to flow seaward along the ocean floor but then turn eastward under the influence of the Coriolis force.

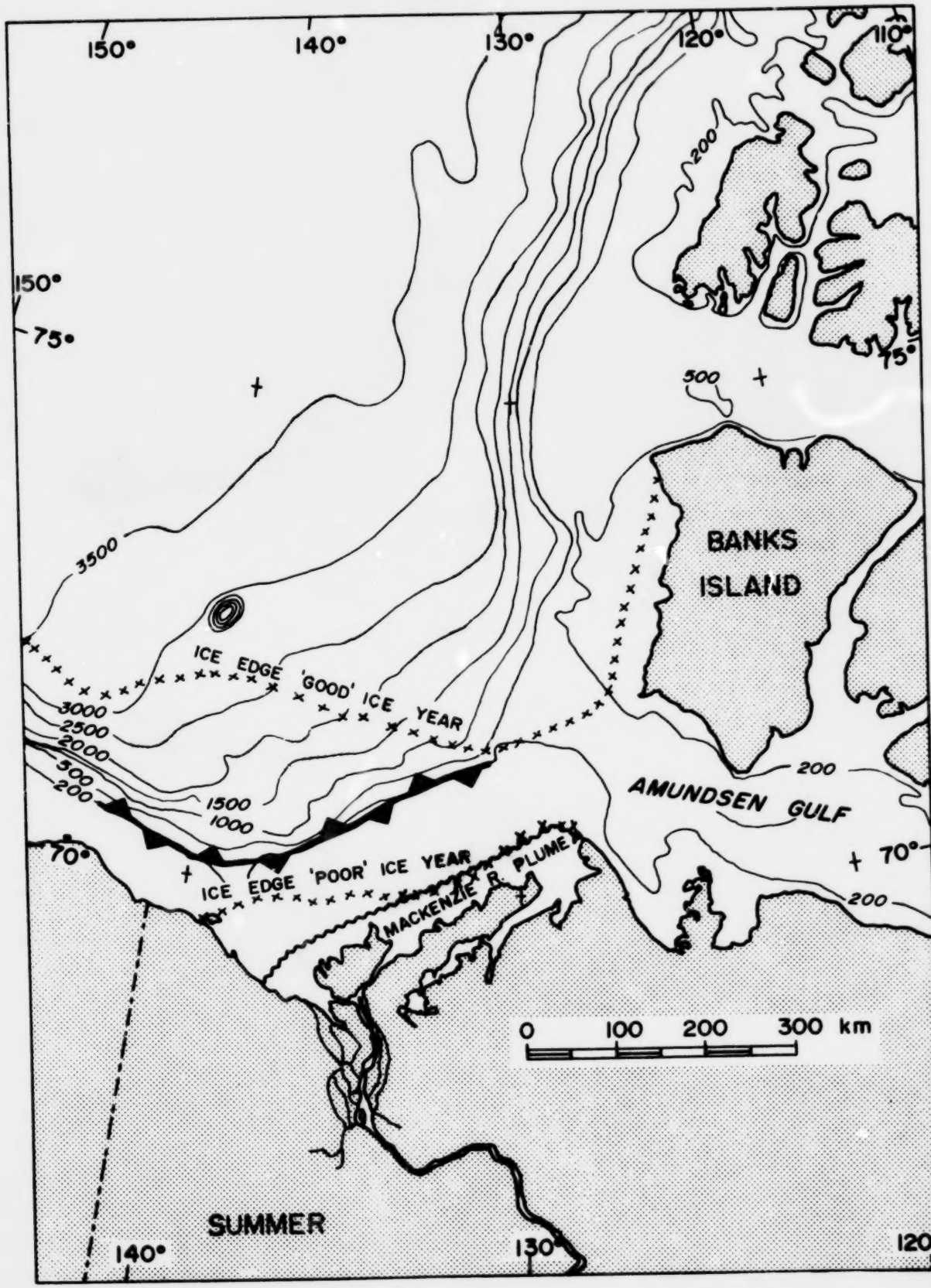

Figure 3.2 Reference Chart for the Southeastern Beaufort Sea

The characteristics of the ice distribution in the Beaufort Sea is important for both offshore and nearshore operations. The seasonal ice conditions are well summarized by Markham (1975). Included on Figure 3.2 is the approximate extent (by late August) of the polar pack ice edge, for both a "good" and "poor" ice year (see Markham, 1975). The presence of ice influences the depth and mixing characteristics of the Mackenzie River plume, results in a regional change of wind stress which could contribute to local surface layer divergences or convergences and limits fetch lengths thus affecting wind-driven currents and wave climate. Freezing and melting of the ice results in local and, at times intense, vertical mixing. Some of these aspects will be discussed in later sections. On a larger scale, ice formation on the shelves is important to the overall circulation in the Mackenzie shelf and slope due to thermo-haline driving. It may also prove important for the heat budget of deep waters, as suggested by Melling (1983), as the cold, salty water left behind during freezing is transported offshore to depths where mixing with the warmer, deep Atlantic Water can occur.

3.2 Mean Seasonal Density Distribution

The density of seawater at a specific location is dependent on both temperature and salinity characteristics of a parent water mass and reflects any mixing with other waters that have occurred. The mean vertical density profile, particularly in the top 200 meters, is a response to changes in the relative amount of mixing and stabilizing influences in the water column. The stratification due to solar heating and fresh water input vary on both a seasonal and geographic basis. The relative contribution of solar heating decreases with increasing latitude while that of salinity decreases with distance from a fresh water source such as a river or ice melt. Mixing forces can be considered to vary seasonally (for example vernal cooling in the fall, salt extrusion during ice formation), but certain processes, such as influences of bathymetry, are independent of season. A review of the seasonal horizontal surface density patterns and vertical density profiles for all Canadian coastal waters was performed by Juszko et al., (1983). The following summarizes the results from that study.

3.2.1 Atlantic Coast

Figures 3.3 (a to d) contain representative vertical density profiles for the Labrador Shelf, Grand Banks, Gulf of St. Lawrence and Scotian Shelf - Gulf of Maine regions, respectively. Table 3.2 summarizes the temperature - salinity - density characteristics of the various water masses found in these areas.

Waters on the Labrador Shelf have a cross-shelf distribution in the summer as shown in Figure 3.4 (see Huntsman et al., 1954). The shelf waters associated with the Labrador Current are characterized by temperatures less than 2°C (to a minimum of -1.77°C), salinities less than 34.4 °/oo (down to 32.5 °/oo) and densities of 26.5 to 27.3 σ_t . In the Central Labrador Sea, the water is relatively homogenous in density beween 27.7 and 27.8 σ_t from the surface to 1800 m.

Progressing southwards, surface waters will be warmed to a much greater extent, and summer surface densities will be reduced. On top of the Grand Banks, the relatively shallow depth allows for uniform mixing, by wind and convective overturning, to the bottom in the winter. The largest stratification occurs in September as both the maximum temperatures and minimum salinities occur simultaneously. The lowered salinities reflect the freshwater pulse carried by the Labrador Current (see Keeley, 1981, for review of seasonal patterns). Along the Tail

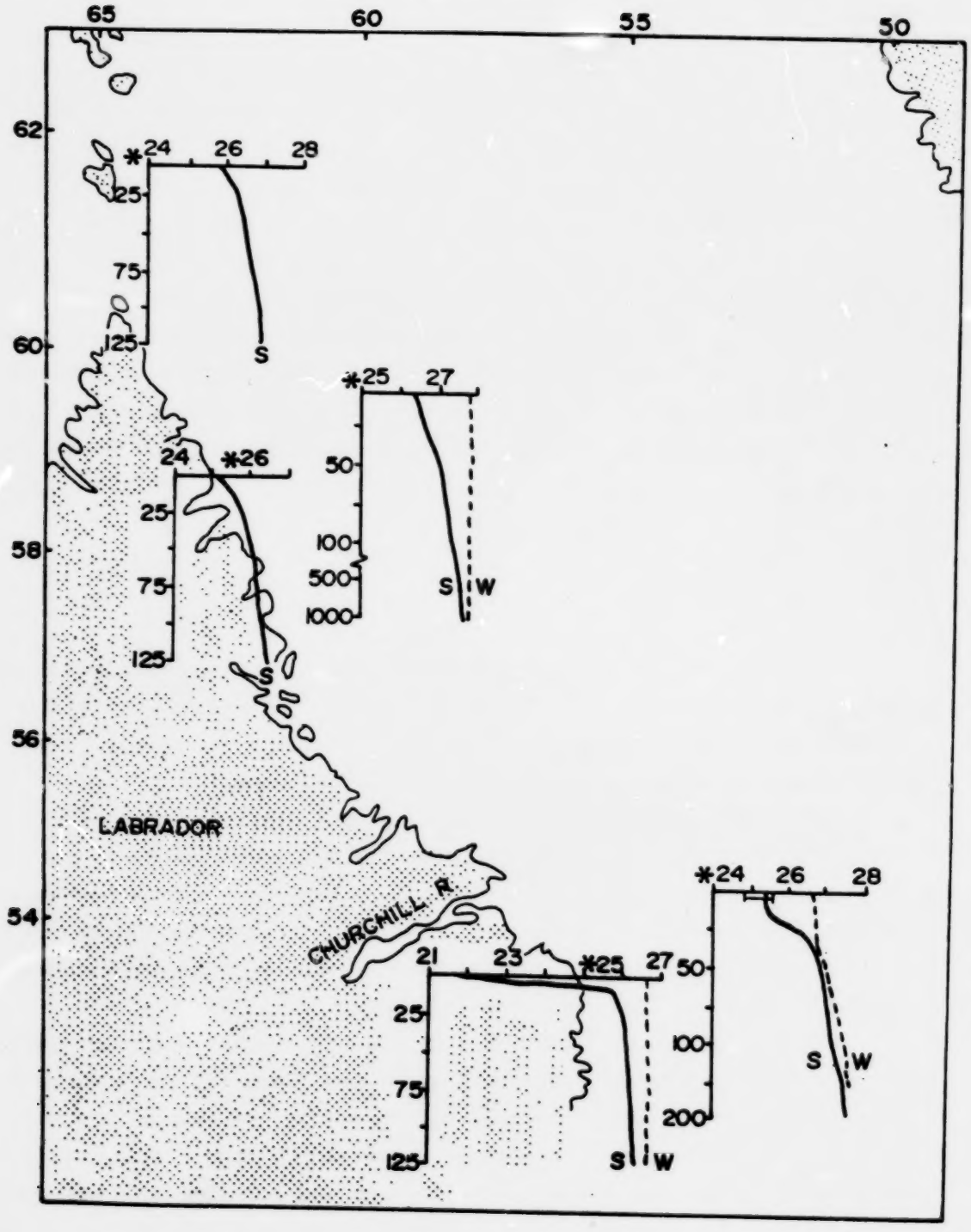

Figure 3.3 (a) Representative vertical density profiles on the Labrador Shelf (from Juszko et al., 1983)

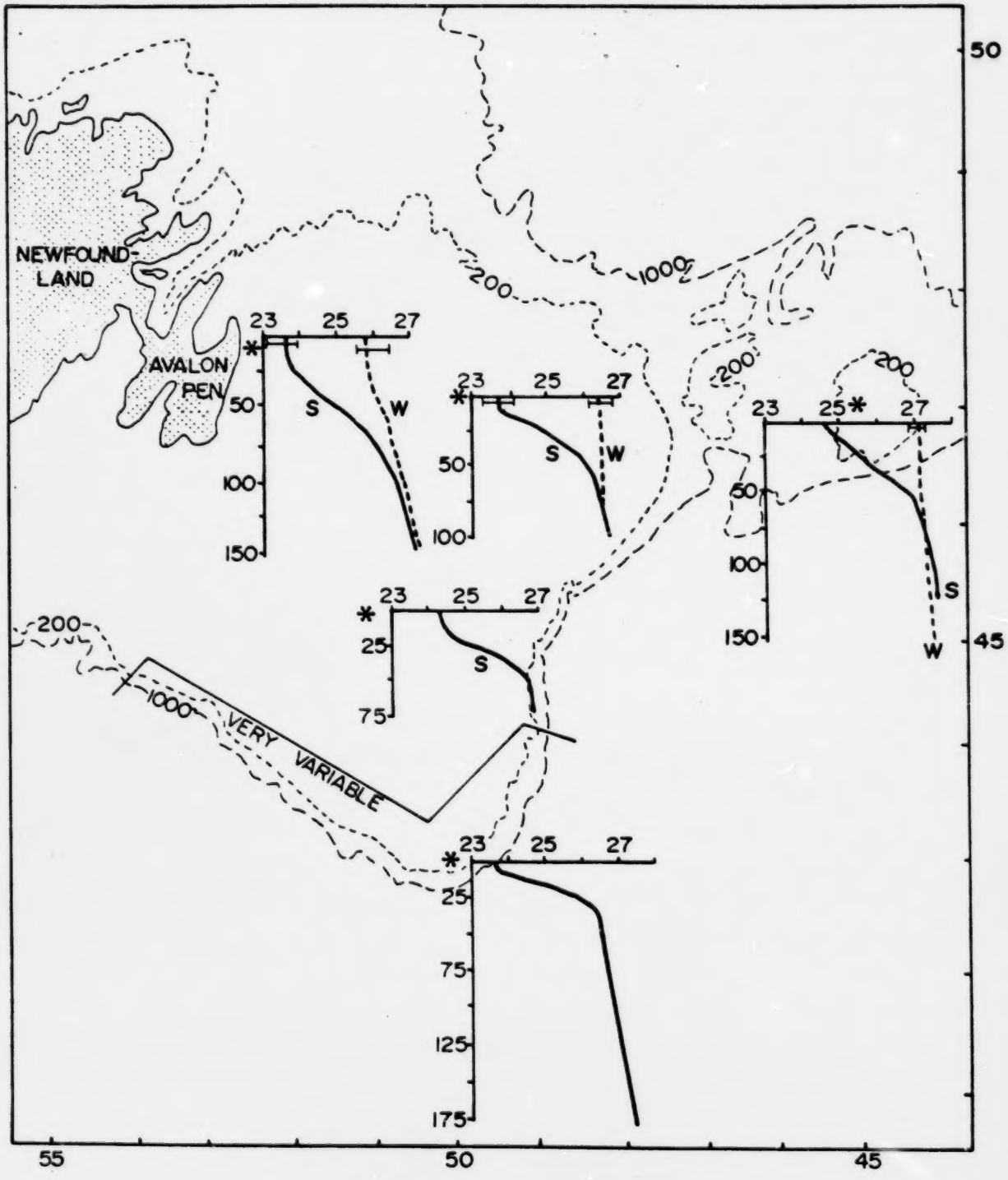

Figure 3.3 (b) Representative vertical density profiles on Newfoundland's Grand Banks (from Juszko et al., 1983)

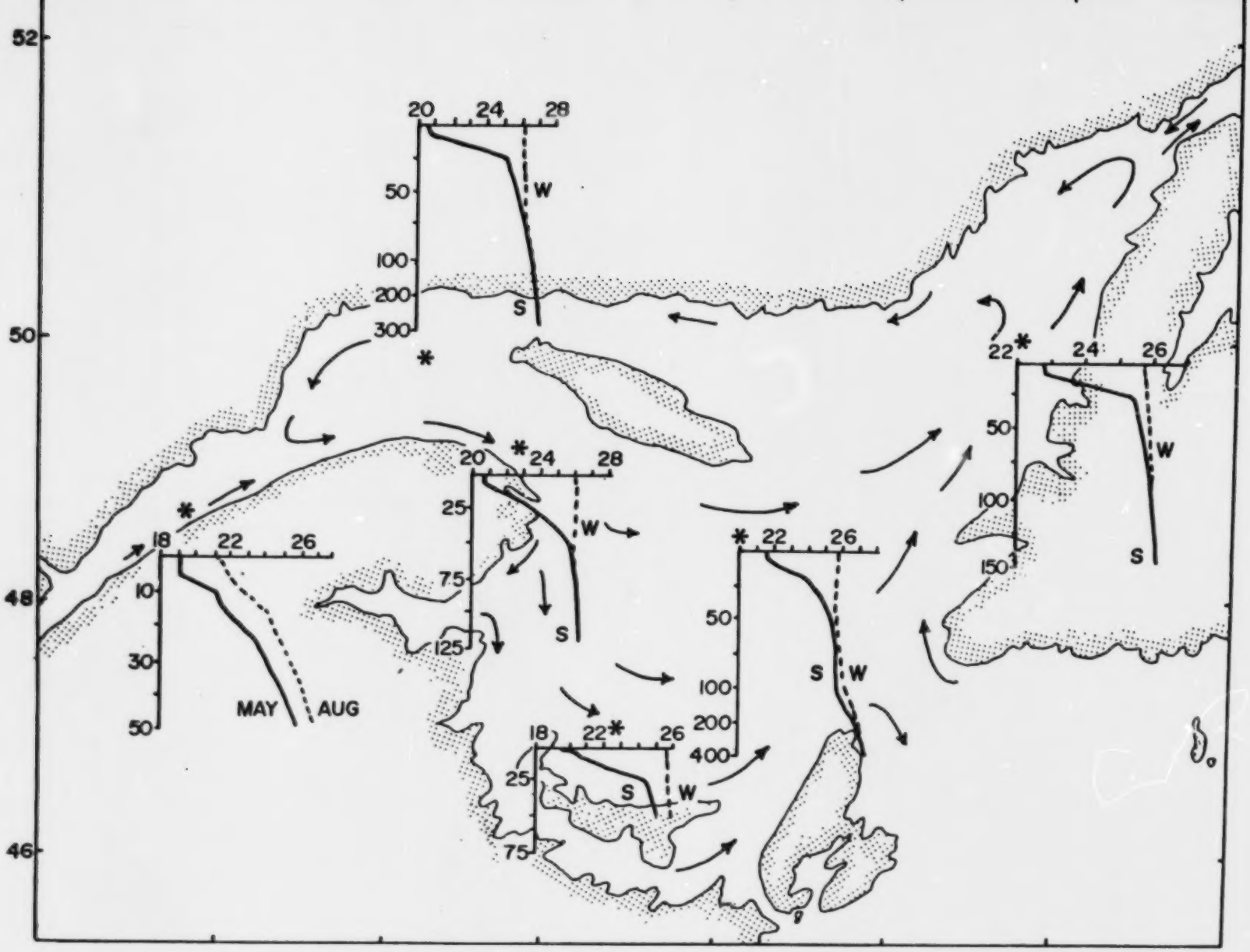

Figure 3.3 (c) Represenative vertical density profiles for the Gulf of St. Lawrence (from Juszko et al., 1983)

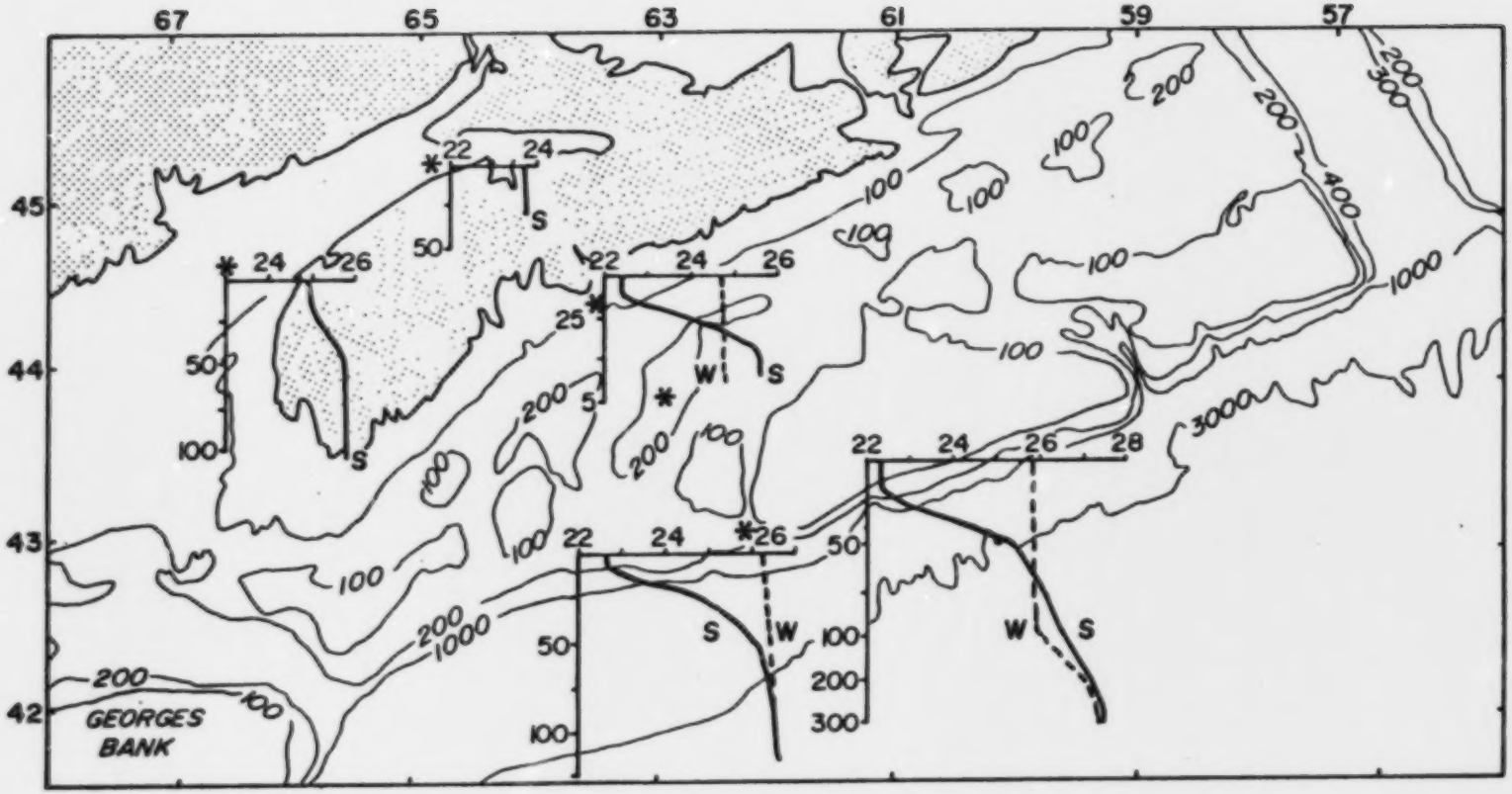

Figure 3.3 (d) Representative vertical density profiles for the Scotian Shelf and Gulf of Maine (from Juszko et al., 1983)

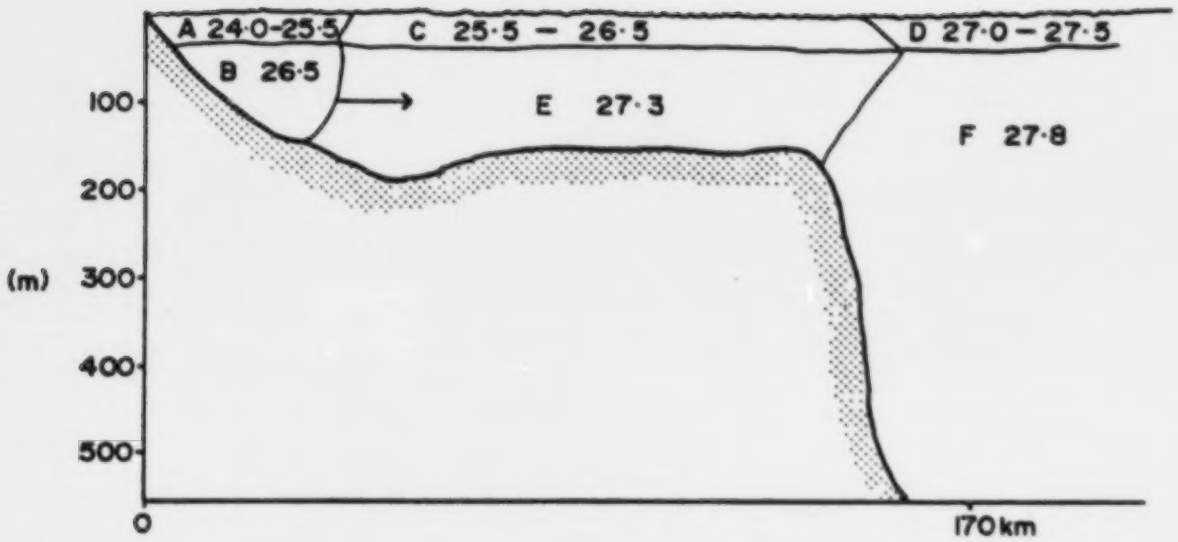

Figure 3.4 Cross-shelf density distribution on the Labrador Shelf (Summer) (from Juszko et al., 1983)

LABRADOR SHELF - SUMMER

- A Surface Labrador coastal water (4.5-6.5° C, < 32.2°/oo)
- B Inshore Branch of Labrador Current (-1.0° C, 32.5-33.4°/oo, winter -1.77° C, 33.1°/oo)
- C Surface water
- D Surface offshore water (3-6° C, 32.5-34°/oo)
- E "Labrador Sea Water" (0-2° C, 33.4-34.4°/oo)
- F Deep offshore water - Labrador sea water modified by the West Greenland Current (> 3° C, > 34.5°/oo)

Table 3.2

Summary of Temperature-Salinity-Density Properties

Area	Water Mass	Season	Temperature °C	Salinity °/oo	Density σ_t
Labrador Shelf	Surface Coastal	Summer	4.5 - 6.5	< 32.2	24 - 25.5
	Inshore Branch Lab. C.	Summer	<2.0 (min. -1.0)	32.5 - 33.4	∿ 26.5
		Winter	mn. - 1.77	∿ 33.1	26.5 - 27
	Surface Shelf	Summer	3 - 6.5	32.2 - 33	25.5 - 26.5
	Surface Offshore	Summer	3 - 6	33.5 - 34.5	27 - 27.5
	Labrador Sea Water		0 - 2	33.4 - 34.4	∿ 27.3
	Deep Offshore Water		3 - 4	> 34.5 - 35	∿ 27.8
Top of Grand Banks	Mixed	Winter	< 0.0	∿ 33	26 - 27
	Surface	Summer	13 - 14.0	∿ 31.75	23 - 24
Gulf of St. Lawrence (Central)	Gulf Surface Water	Summer	10 - 16	31 - 32	22 - 24
		Winter	< 0 (min. -1.7)	32 - 32.5	25.8 - 26.5
	Gulf Intermediate Water	Summer only	< 1.5 (min. -1.0)	32 - 33.5	25.5 - 26.5
	Deep Gulf Water		3 - 5	33.5 - ∿34.2	26.5 - 27.2
Scotian Shelf	Surface Layer	Summer	17 - 19	31 - 32	22 - 23
		Winter	1 - 3	31.5 - 33	∿ 26.0
	Intermediate Layer	Summer	4 - 5	32 - 33.5	25 - 26.5
	Deep Layer (Basins)	Summer	5 - 8	33.5 - 35	26.5 - 27.2
		Winter	4 - 5	33 - 34.0	26 - 27
Warm Core Ring	Sargasso Sea Water		> 20 (at surface)	36 - 36.5	25 - 27

of the bank, conditions can be quite variable due to the possible impingement of the Gulf Stream which creates a strong thermal front with Labrador Current water.

In the Gulf of St. Lawrence, the vertical density structure reflects the circulation pattern which determines the relative contribution from summer heating and input from the St. Lawrence River (see Figure 3.3 (c). Note "summer" in this figure represents the maximum stratification that is observed during the year.) In the Upper Estuary, density stratification is controlled by freshwater input counterbalancing vertical mixing in the shallower waters. At the head of the Laurentian Trough, mixing is also occurring due to internal wave activity and upwelling. The maximum stratification occurs in May associated with the river discharge peak. Horizontal density gradients can occur between the estuary and Central Gulf region. In the spring, the lower estuary is freed of ice prior to the central Gulf and surface waters can warm up creating as much as a 6°C difference. In late summer, surface waters in the estuary may be cooler due to upwelled and advected subsurface waters. The reduced water depth in the Magdalen Shallows allows for uniform mixing to the bottom in the winter ($\sim 25.8\sigma_\theta$). Maximum stratification (or minimum surface density) occurs twice in the summer, once at the beginning of July due to fresh water input from the estuary and again in mid-August when surface temperatures are maximum ($\sim$ 18°C, densities as low as $19\sigma_\theta$).

The central and northeast Gulf waters are influenced primarily by heating as most of the fresh water outflow is constrained over the Magdalen Shallows. The water column has a distinct three layer structure in the summer with a surface mixed layer 10 - 20 m deep, a cold intermediate layer between 50 and 100 m and delimited by the 1.5°C isotherms, and a deep, warmer, saline layer. The Gulf Intermediate Layer is remnant cold, winter water, while the Deep Layer results from inflow through Cabot Strait. In the winter, the surface layer extends to 100 m deep with densities between 25.8 and $26.5\sigma_\theta$. Water properties in the Northeast Gulf may also be affected by inflow from the Strait of Belle Isle which provides colder and fresher water along the north shore. Depending on the flow conditions, both Cabot Strait and the Strait of Belle Isle will contain fronts separating the inflowing and outflowing water.

Various factors are operating on the Scotian Shelf and in the Gulf of Maine which result in the observed density distributions (figure 3.3 (d), 3.5 (a), (b)). In the summer, a three layer system in temperature, with a corresponding two layer system in density, is present on the Scotian Shelf. The surface waters are derived from the Gulf of St. Lawrence with the fresh water pulse reaching Cape Sable by December -

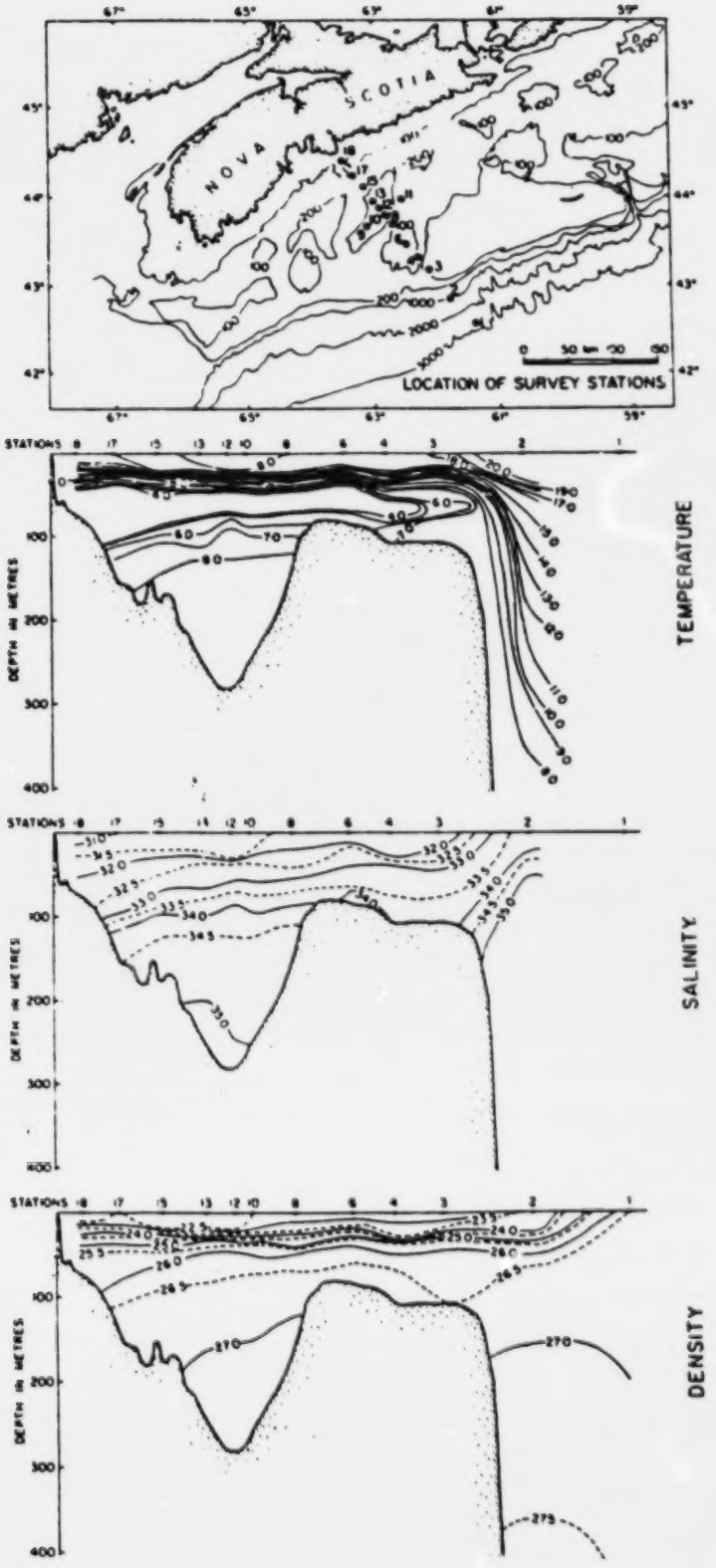

Figure 3.5 (a) Cross-shelf property distribution at the Halifax Section (Summer - from de La Ronde (1972))

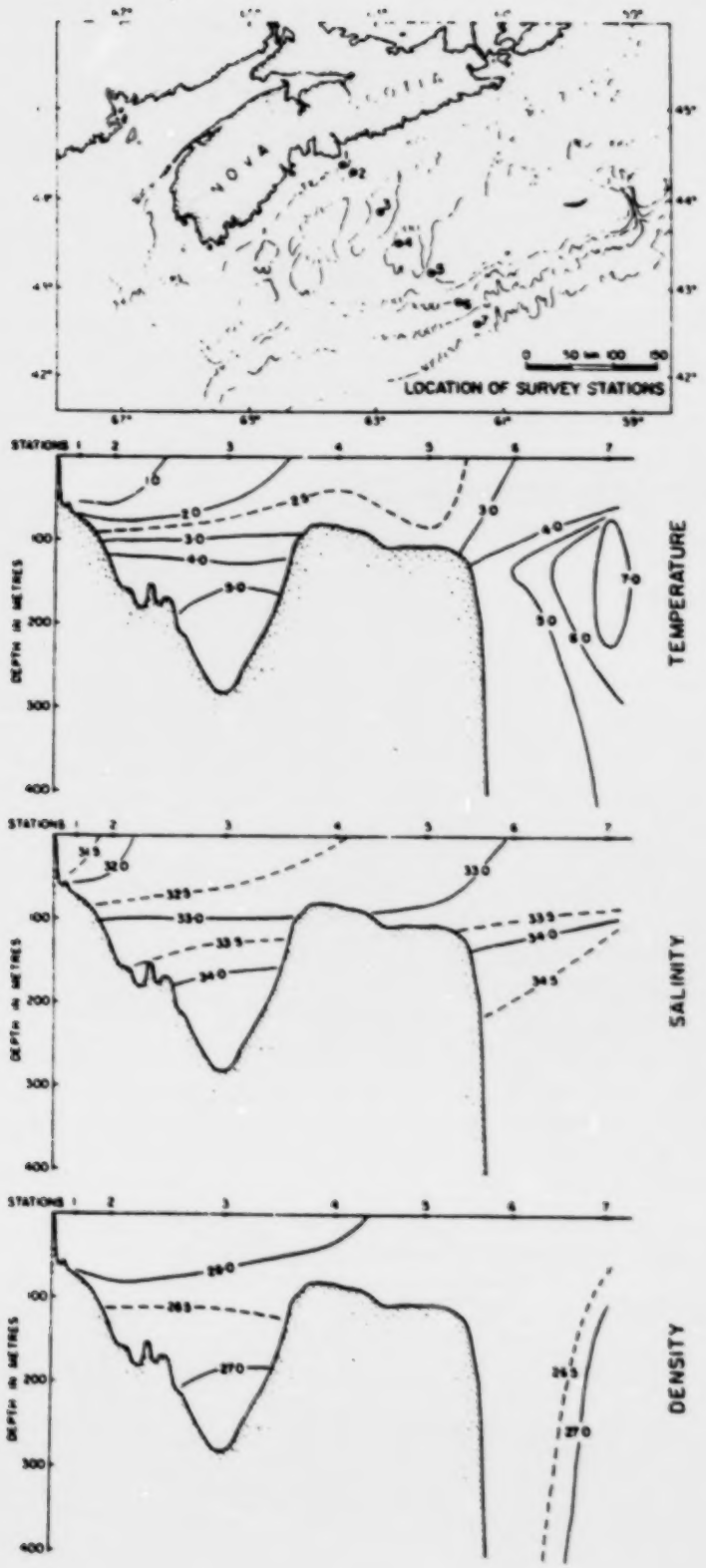

Figure 3.5 (b) Cross-shelf property distribution at the Halifax Section (Winter - from de La Ronde (1972))

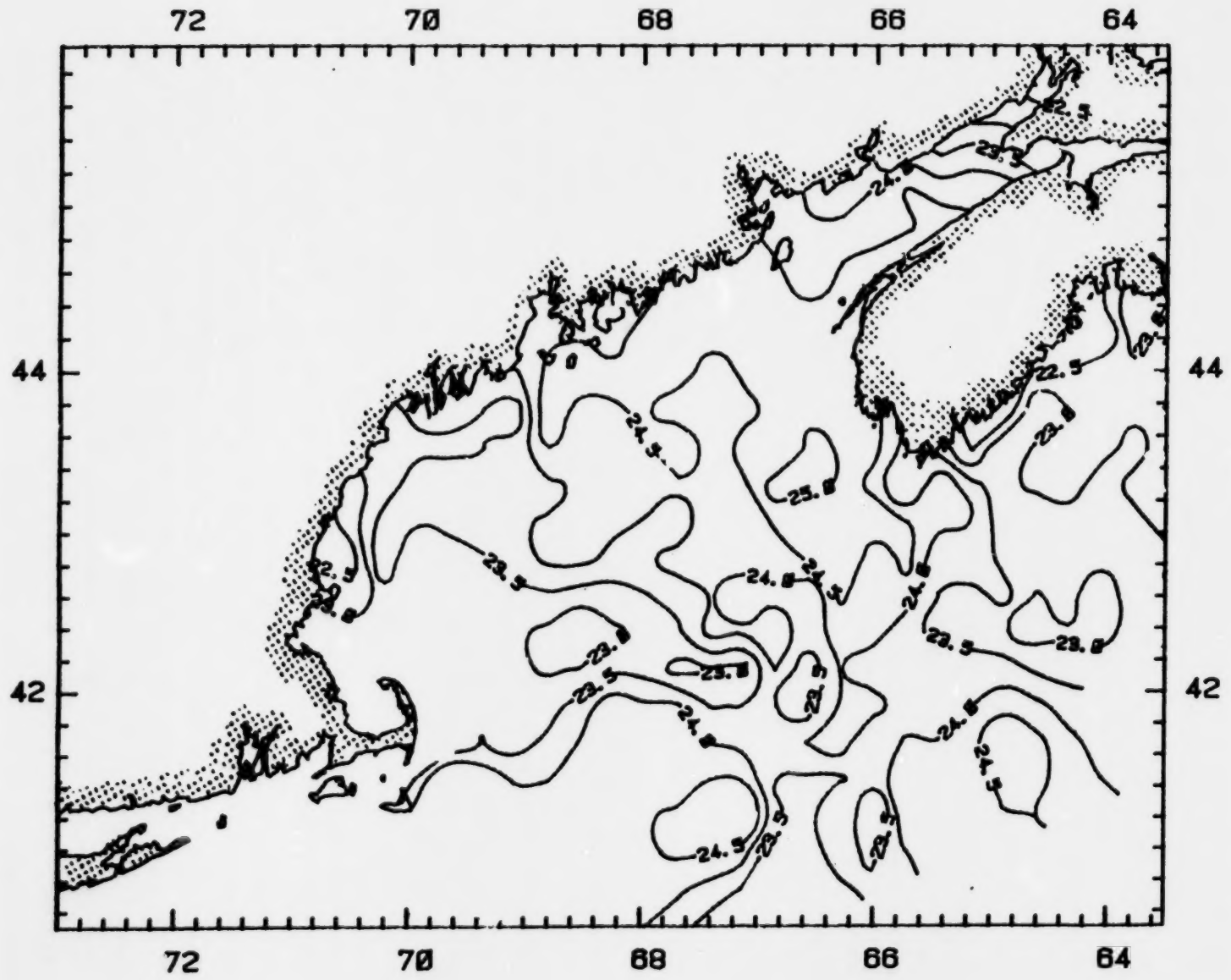

Figure 3.6 Contoured surface densities in the Bay of Fundy and Gulf of Maine - Summer (from Juszko et al., 1983)

January (Sutcliffe et al., 1976). The cold, intermediate water is considerably modified Labrador current water and not a remnant of winter cooled waters. The bottom layer is slope water that has penetrated onto the shelf. In the winter, nearshore and on top of banks, the water column may be completly mixed to the bottom. Over the continental slope, surface waters show salinity and temperature increase offshore reflecting the mixing between shelf water and the Gulf Stream. Below 200 m, water is a mixture of Labrador and North Atlantic Central Water ($\sigma_t > 27$) (Gatien, 1976). A shelf-slope front exists permanently near the shelf break while a second front corresponds to the northern edge of the Gulf Stream. In the Bay of Fundy - Gulf of Maine area, stratification is generally a compromise between the stabilizing effects of solar heating (summer) and vertical mixing due to tides. In the central Gulf of Maine, the summer vertical profile again consists of three layers with a cool, intermediate layer from 50 to 150 m (2 - 5°C, 32 - 32.5 °/oo, 25.3σ_t) as remnant winter mixed water and the deep layer (6°C, 34.5 - 35 °/oo, 27.2σ_t) representing intrusion of slope water through the Northeast Channel. In the winter, the surface layer extends to 150 m (1 - 2 °C, 32 °/oo, 25.8σ_t). The upper reaches of the Bay of Fundy resemble a "well-mixed" estuary due to the strong tidal mixing. Changes in the horizontal density pattern can be observed over a tidal cycle. The cyclonic circulation pattern results in a decrease in density across the Bay of Fundy towards the New Brunswick shore. This can be seen in Figure 3.6 as well as areas of increased density over Georges Bank and off the tip of Nova Scotia due to vertical mixing.

3.2.2 Southeastern Beaufort Sea

The water column in this region can be considered as a two layer system with Arctic Water (σ_t 26) above 250 m and Atlantic Water below. The Arctic layer is often subdivided into two: the Arctic Surface layer (upper 5 - 50 m) which is directly influenced by atmospheric forcing and the Arctic Subsurface Layer (down to 0°C) which encompasses most of the pycnocline (Melling, 1983). In the area of interest, both the vertical and horizontal density distribution is controlled by salinity changes in the upper 20 metres, related to Mackenzie River discharge (peak in May -June) and the relative position of the polar pack ice. The Mackenzie River plume is confined to the upper 5 - 20 m and generally within 30 - 50 km of shore though its position is dependent on wind conditions which can push the plume away or towards the shore. The polar pack can also act as a barrier to the offshore extent of the plume as can be

seen in the difference in surface density over the shelf during poor or good ice years. For example, in 1974 (poor ice year), summer surface water densities were less than 5 σ_t over the entire shelf while in 1975 (good) they ranged from 8 to 22σ_t, increasing offshore. In the winter, the upper 50 meters are generally mixed to a uniform density close to 26σ_t. Under the landfast ice, the reduced river flow results in a shallow, 3 -5 m brackish layer near shore. Variations at synoptic periods are super-imposed on the seasonal variations in river discharge (Fissel and Birch, 1984). Other areas of reduced surface density can be associated with the melting edge of the polar pack or runoff from icefields.

The Mackenzie River not only influences density structure butit is also the major contributor of sediments to this shelf region. Fissel and Birch (1984) have reviewed the sediment transport processes in this area and have developed a conceptual model to describe it. This has direct implications on oil dispersal due to absorption onto sediments and potential reworking of bottom deposits.

3.3 Topographically Related Features

Ocean coastal boundaries and rapid changes in bathymetry influence both local and large scale dynamics. The transition between continental shelves and the deep ocean is one of the most important areas of water property exchange through 1) boundary layer mixing followed by along-isopycnal advection (ex. Armi, 1978); 2) thermo-haline frontal exchange (ex. see Section 4.2); 3) generation and breaking of internal waves (ex. see Section 4.1); 4) periodic upwelling and downwelling; and 5) catastrophic events such as Gulf Stream ring entrainment (see Section 3.4). Fronts are often associated with changes in bathymetry. On the Scotian Shelf/Slope, three frontal regions can be identified. The first lies offshore and is associated with the north wall of the Gulf Stream, a region of steeply sloping isopycnals and strong current shear. Its position reflects both the mean position of the Gulf Stream as well as any meanders that are present. At the shelf/slope boundary, a thermo-haline front exists, with little horizontal change in density (Horne, 1978; Section 4.2). Circulation in this region has recently been investigated by Smith and Petrie (1983) from direct current measurements. They found that cross-shelf currents, especially at the surface, showed an annual signal with mean surface flow offshore which peaked in the winter ($\sim$ .1 m/sec). This could reflect a possible Ekman transport in the surface layer, in response to the annual signal in longshore winds, however they could not balance the large transport with either return flow in deeper water (observed onshore around .02 m/s) or the relative stationarity of the shelf/slope boundary without assumptions on longshore gradients or cross-frontal exchange. Indirect evidence of deep onshore flow is the presence of slope water in the deeper basins on the shelf (see Section 3.2). The alongshore flow in the deep waters of the slope was towards the west, at .01 - .02 m/sec, while surface alongshore flow showed variability at subtidal synoptic periods (2 - 10 days) as well as ocean forcing periods (10 - 90 days) related to the low frequency displacement of the shelf/slope water boundary. The net surface flow was eastward, with speeds up to .15 m/sec.

The third type of front present in the Scotian Shelf - Gulf of Maine region is termed a tidal-mixing front (see Figure 3.1). Simpson and Hunter (1974) initially discussed these fronts and associated them with the boundary between stratifying effects due to solar heating being dominant over vertical mixing induced by bottom shear of the tidal currents. This relationship is parameterized by the well known, BH/u^3 criteria, where **B** is the buoyancy flux due to heating, **H** is the local water depth and **u** is an estimate of tidal velocity. This analysis has been extended to the

Bay of Fundy and Gulf of Maine by Garrett et al. (1978) where the transistion from well-mixed to stratified conditions in the summer occurs for values of $H/u^3 \sim 70\ m^{-2}\ s^3$. The dynamics and characteristics of these fronts will be discussed in Section 4.2

Wind-driven upwelling has long been known to occur along coasts as well as at the shelf break. Alongshore winds, with the coast on the left looking downwind (in the northern hemisphere) causes a divergence in the surface layer, which by continuity requires an upward transport of subsurface waters. This is generally an intermittent feature but has been observed, for example, along the North Shore of the Gulf of St. Lawrence (Trites and Walton, 1975) and on the Beaufort Sea Mackenzie River Shelf (Fissel, 1981). Areas of persistent upwelling not associated with local winds have also been identified. One of these is at the head of the Laurentian Trough associated with the entrainment of deeper waters into the outflowing surface layer. Observations of sea bed drifters by Lauzier (1967), identified two persistent areas of bottom onshore flow, one off of Louisbourg (Cape Breton Island) and the other around the southern tip of Nova Scotia off Yarmouth. Onshore velocities in this latter area were on the order of .005 - .02 m/sec. Garrett and Loucks (1976) suggested a mechanism of centrifugal upwelling whereby the centrifugal force required to turn the strong tidal current (O (1 m/s)) around the tip of Nova Scotia is balanced by a pressure gradient positive offshore. In the bottom boundary layer, the tidal current will be reduced due to friction and the pressure gradient here is unbalanced resulting in a net shoreward drift. Recent current and water property measurements in the area have led Smith (1983) to discount this force balance as the main driving term and to suggest upwelling driven by the longshore density variations which are maintained by tidal mixing. Evidence for this lies in an observed seasonal signal in the near-bottom cross-isobath current, with a maximum occurring in summer when horizontal stratification change would be the most important, and an offshore flow driven by tidal rectification, opposite to centrifugal upwelling. Smith (1983) also showed that the majority of the coastal circulation lies in a narrow band within the 110 m isobath with a distinct seasonal signal having a winter peak (.06 - .10 m/s) which carries the fresh water pulse originating in the Gulf of St. Lawrence (average transport into the Gulf of Maine of $.14 \times 10^6\ m^3/s$). A closed, anti-cyclonic gyre, with velocities .05 - .15 m/s, existed around Brown's Bank.

The interaction of oscillating currents with bottom topography can create a mean flow which is particularly pronounced in regions of large tidal velocities. The rectified, along-isobath current results from a divergence of the tidal Reynold's stress which is balanced by bottom friction. In a depth-dependent model, Loder

(1980) accounts for the current jet observed on the North Slope of George's Bank through this mechanism. Zimmerman (1978), through a perturbation analysis of the potential vorticity equation around small bottom topography, showed that maximum rectification occurs when the horizontal length scale of the bottom topography matches the tidal excursion. Recently, Loder and Wright (1985) have included vertical dependence in the Loder (1980) model by introducing a vertical eddy viscosity. They show that the expected cross-isobath motion on the side of Georges Bank consists of circulation cells which could account for upwelling in the region. Furthermore, they also show that the mean Lagrangian velocity may be in the opposite direction to the mean Eulerian current which implies that the mean flow recorded by current meters would not reflect individual water parcel motion.

3.4 Macroscale Waves and Eddies

The behaviour of macroscale waves is related directly to the conservation of vorticity either through variation in latitude (i.e., in a β-plane) or through vortex stretching over a mean bottom slope. The latter is important over continental slopes and these waves are termed topographic Rossby waves. They have been observed on the Scotian slope through an examination of longshore currents at the shelf/slope boundary (SSB) by Smith and Petrie (1982) and Louis et al. (1982). Their signature is seen as bursts of 3 or 4 oscillations with periods ranging from 15 to 30 days and speed variations of .10 - .20 m/sec, both of which are modulated. The forcing is by the radiation field of a warm-core Gulf Stream ring travelling over the continental rise (Louis et al., 1982). The presence of Gulf Stream rings or meanders of the Gulf Steam will also influence the position of the shelf-slope boundary moving it further on or off the slope. From a space-time autocorrelation of the digitized position of the SSB over three years, Smith and Petrie (1982) calculated a net westward propagation of SSB fluctuations of 4.6 km/day with a temporal scale around 4 weeks and a spatial scale of 140 kms.

Gulf Stream rings are formed by meanders of the Gulf Stream which eventually pinch off to leave an isolated ring of current within which is trapped Sargasso Sea water (i.e., "warm-core") to the North or slope water (i.e., "cold-core") to the South of the Gulf Stream. Approximately 5 to 8 rings of each type are formed per year, with 2 - 3 warm core rings present at any one time in the slope waters (see Lai and Richardson, 1977, Ring Group 1981). These rings translate westward at 1 to 5 kms/day until they reach Cape Hatteras where they are reabsorbed by the Gulf Stream. Warm-core rings range from 100-200 kms in diameter, have a rotational velocity as high as 1.5 m/sec, are characterized by a downward displacement of isotherms seen as deep as 1500 meters and contain a layer of uniform warm water up to 600 m deep. Cold-core rings are larger, 150 - 300 kms in diameter, and can extend to the sea floor (4000 - 5000 meters). Both types can transport up to ten thousand cubic kilometers of water as they translate westward. Decay of the rings acts essentially as a mixing mechanism across the boundary set up by the strong current shear of the Gulf Stream. Warm-core rings, as discussed earlier, can contribute to the variability observed at the shelf/slope boundary along the Scotian Shelf and may also act to remove coastal water from the shelf onto the slope (an entrainment rate of 0.4×10^6 m^3/s estimated by Smith (1978)). Their somewhat catastrophic influence may prove important when tracking any tracer including spilled oil.

4. MESOSCALE FEATURES

4.1 Mesoscale Waves

The mesoscale waves of particular interest are internal waves with frequencies ranging from inertial and tidal to the local Brunt-Vaisala frequency.

If a parcel of water is displaced adiabatically in the vertical and allowed to relax freely, it will overshoot and oscillate about an equilibrium position. Neglecting a slight pressure affect, the frequency of oscillation is given by (see Gill, 1982):

$$N^2 = -\frac{g}{\rho_o}\frac{\partial \rho_o}{\partial z} \qquad 4.1.1$$

where N is the Brunt-Vaisala frequency, **g** the acceleration due to gravity, ρ_o the background time in independent density and $\partial \rho_o / \partial z$ the vertical density gradient. If the water column is forced to oscillate vertically at a frequency other then N, then the waves will propagate away from the source at an angle to the horizontal given by (see Leblond and Mysak, 1976).

$$\tan\theta = \pm \left(\frac{\omega^2 - f^2}{N^2 - \omega^2}\right)^{1/2} \qquad 4.1.2$$

where ω is the driving frequency and **f** is the coriolis parameter. From equation 4.1.2 it is evident that internal waves can exist only in the frequency band of

$$N^2 > \omega^2 > f^2$$

For frequencies outside this range, the motion is diffusive rather than wavelike and disturbances decay away from the source. This discussion assumes a background density structure depending on vertical variations alone. Mooers (1975) has shown that the ray paths given by equation 4.1.2 are modified in the presence of horizontal density structures (fronts). This results in a modification only of the detail of the internal waves.

Two approaches are used to investigate internal waves - that of rays and that of modes. Under the Boussinesq approximation and the assumption of a flat bottom, the horizontal and vertical velocity components decouple and the velocity field can be expressed as a sum of normal modes. Generally, most of the fluctuating energy is contained in the first several modes. Magaard and McKee (1973) used this approach

to describe the semidiurnal tide at site 'D' in the Western North Atlantic. Garrett and Munk (1972, 1975) assuming that background internal wave energy was far from the generation site, have defined a "universal" internal wave spectrum in order to describe the correlation length scales in the ocean. In the presence of bottom topography, the bottom boundary condition couples the vertical and horizontal velocities and a ray path analysis must be used. Petrie (1975) used this approach to describe the M_2 surface and internal tides on the Scotian shelf and slope.

Various mechanisms have been proposed for the production of internal waves. Phillips (1980) has suggested that slowly moving storms may have energies appropriate for their generation. Thorpe (1975) has shown that two surface gravity waves and an internal wave can form a resonant triad. If the sum of the wave numbers and frequencies of two surface gravity waves equals the frequency-wavenumber relationship of an internal wave then existing non-linearities can allow for transfer of energy from the surface gravity waves to the internal wave. The most important mechanism for the generation of internal waves on the continental margins is through interaction of the flow with bottom topography. The particle path of an internal wave corresponds to the propagation angle given by equation 4.1.2. If the bottom slope also corresponds to this propagation angle and the water is forced to oscillate along the slope (by the surface semi-diurnal tide, for example) then intense generation of internal waves will occur. The theory for this production was established by Baines (1972). Marsden (1985) has shown that this production method on Georges Bank results in internal tidal velocities as large as the barotropic tidal velocities (with an estimated horizontal diffusivity of 200 m^2/s due to breaking of these internal tides). Petrie (1975) has shown strong internal tide generation at 200 m depth on the Scotian shelf (with estimates of diffusivities of $K_v = 10^{-2}$ m^2/sec, K_h = 200 m^2/sec).

Internal waves are important in dispersion processes for three reasons. First, they cause internal fluctuations of isopycnals with observed amplitudes greater than 30 m (see Holloway, 1984; for a review of observations of internal waves see Denman and Gargett, 1983). If, for example, oil sinks in a region of large internal wave production, through time it may oscillate over a large part of the water column. Second, the troughs of an internal wave are regions of convergence while the crests are regions of divergence of water (see Thomson, 1981). Hence, the distribution of any sinking or dispersed oil may be non-homogeneous and concentrated in the troughs. Third, internal waves can break causing intense mixing. Turner (1979) has shown that internal waves break while travelling from stratified to unstratified regions or

where internal waves propagate up a slope into shallow water. Marsden (1985) suggests that breaking internal waves on Georges Bank may contribute significantly to the cross-isobath scalar fluxes in the region. Finally, Gargett and Holloway (1984) suggest that the vertical eddy diffusivity for mass due to internal wave breaking may be obtained according to a $K_v \propto N^{-1.0}$ or $K_v \propto N^{-0.5}$ relationship where **N** is the local Brunt-Vaisala frequency.

4.2 Frontal Features - Dynamics and Cross-frontal Exchange

Frontal regions are best examined through a discussion of the physical processes involved in frontogenesis (i.e., frontal formation and maintenance) and in cross-frontal exchange leading to potential breakdown of the front.

The dynamics of shallow sea fronts were reviewed by Garrett and Loder (1981). Shallow sea fronts are formed where there is a horizontal gradient in the relative contribution of stabilizing (such as solar heating) and mixing forces (such as bottom friction on tidal currents) acting on the water column. Much of the original work was performed on fronts observed near England (ex., Simpson, 1981). These fronts are characterized by an abrupt change in stratification, a position predicted by the H/u^3 parameter, strong along-front flows ($\sim$ 0.2 cm/sec) and the presence of instabilities leading to perturbations along the front (wavelengths of 20 - 40 kms) which can break off and transport large amounts of water across the front (Simpson, 1981). The along-front flow is consistent with a geostrophic current however their predictions, using the observed density gradients, are often larger than measured. Simpson (1981) suggests that the simple energy balance leading to the H/u^3 criteria may not be sufficient to account for all the observations including the lack of shifts in frontal position over spring-neap tides, the complicated current patterns and baroclinic instabilities.

Frictional flow at the front was suggested by Garrett and Loder (1981) as one mechanism for frontal circulation. In this case, the horizontal diffusion rate of an isopycnal is given by the local value of $(N^2 / f^2)\ \nu_v$ where N is the Brunt-Vaisala frequency, f, the coriolis parameter and ν_v the eddy viscosity. Maximum lateral diffusion occurs on the stratified side thereby weakening the front on the less dense side and sharpening on the denser sider (i.e., convergence). The decay time of the front, assuming density advection balanced by vertical diffusion (K_v) was shown to be $(N/f)(\nu/K_v)^{1/2}$. A model for the tidal front on Georges Bank, over sloping bottom, showed a circulation dependent on a Ekman number ($E_k = \nu_v\ (f\ h^2)^{-1}$) which varies horizontally across the front, increasing on the well-mixed (denser) side. A two-cell circulation pattern develops here with surface convergence, downwelling along the frontal interface and upwelling along the bottom of the well-mixed side. The model involves a parameterization of a vertical eddy viscosity as $\nu = \nu_0\ F(R_i)$, (i.e., function of an average Richardson number) with ν_0 given by $u_*^2/200f$ (u_* average friction velocity of the tidal current, see Csanady, 1976).

Mixing across shallow-sea fronts can occur by numerous processes including mean flow across the front, shear dispersion (similar to tidal estuaries), baroclinic eddies and simply by changes in the frontal position, increasing or decreasing the extent of the well-mixed side. Away from the surface and bottom Ekman layers, for low Ekman number fronts a cross-frontal mean flow can be obtained assuming a geostrophic balance to the sloping isopycnals. The cross-frontal velocity has the form

$$u \simeq -g f^{-2} \frac{\partial}{\partial z} \left(\frac{\nu_v}{\rho_0} \frac{\partial \rho}{\partial x} \right)$$

By continuity, the vertical velocity is given by

$$w \simeq g f^{-2} \frac{\partial}{\partial x} \left(\frac{\nu_v}{\rho_0} \frac{\partial \rho}{\partial x} \right)$$

(Garrett and Horne, 1978; Garrett and Loder, 1981), which leads to downwelling on the denser side. Baroclinic eddies have been observed by satellite photos for both the Celtic seafronts and around Georges Bank (radius here $\sim$15 kms).

Shelf-break fronts are retrograde fronts as defined by Mooers et al. (1978) having a cross-frontal scale of the order of the internal Rossby radius of deformation, an along front scale of many radii and a persistence greater than several inertial periods. The shelf-slope front off Nova Scotia is generally less than 10 kms wide (1 to 20 kms) and characterized by strong interleaving of water masses with the layers coherent for several kilometers along the front, extending the width of the front, and having depths of 10 - 20 meters (Horne, 1978). The strong gradients in temperature are compensated by changes in salinity across the front resulting in little density signature. Within each interleaving layer, the density is homogenous so that a vertical density profile has a characteristic step-like appearance. Along the upper and lower boundaries of these layers, mixing (on scales .01 to 1 m) occur due to double diffusive processes (see Turner, 1973, Chapter 8 for a good discussion). Double-diffusion results from the unequal molecular diffusivities of heat and salt. If cold-fresh water lies over warm-salty water, a temperature driven "diffusive" mixing occurs as heat diffuses faster than salt, and at the boundary, convective motion in

both layers is set-up. If warm-salty water lies over cold-fresh, salinity driven mixing occurs and a salt-finger interface develops. Double diffusive transports cause the intrusive layers to lose their temperature and salinity anomalies and to change density, either rising or sinking depending on the relative fluxes from the upper and lower surfaces. Assuming a balance between cross-frontal advection of heat and salt into an interleaving layer and diffusion by small scale "double-diffusive" mechanisms, Horne (1978) estimated a lifetime of approximately 30 hrs for a layer extending 3 kms, an intrusive velocity of .03 m/sec with a corresponding horizontal diffusivity of K_h = 260 m^2/sec and vertical eddy diffusivity in the frontal zone K_v = 5-50 X 10^{-4} m^2/sec. Mixing due to cabbeling (i.e., the formation of denser water by the mixing of two waters of equal density but different temperature and salinity) could result in a downwelling velocity of 1 - 10 m/day, possibly contributing to the maintenance of the front (Garrett and Horne, 1978; Horne et al., 1978). Calving of the shelf slope front off the mid-Atlantic Bight has been observed (Mooers et al., 1978) and may also be occurring off Nova Scotia. Here lens shaped parcels of water (10 - 20 kms wide, 20 to 50 m thick) are transferred from the shelf to the slope, with a seaward migration along isopycnal surfaces. The front is also subject to instabilities, internal tide oscillation, and impingement of Gulf Stream rings as discussed in section 3.3.

Large scale interleaving has been observed in the Beaufort Sea shelf/slope (Melling, 1983) due to the cold, salty waters, formed on the shelf by water freezing and salt extrusion, which can come into contact with the warmer Atlantic waters, at depth, off the shelf. Though so far not studied, many of the processes observed off the Scotian shelf should be occurring here as well.

River plume fronts (ex. Mackenzie River) have the general characteristics described by Bowman and Iverson (1978) and modelled by Garvine (1980). River plume fronts always show a two sided convergence and downwelling. The front spreads relative to the ambient fluid driven by the horizontal pressure gradient of the river water and oppositely directed interfacial slope. Surface waters are entrained and mixed downwards, opposite to the upward entrainment in estuaries. Along the outer edge of the Mackenzie River plume, eddies, as observed in satellite photos, can break away from the plume and act to mix the brackish nearshore water with that overlying the continental shelf (Fissel and Birch, 1984). These would be a result of instabilities similar to those of other fronts.

There has recently been increased interest in mixing caused by melting icebergs and glaciers. Laboratory experiments (ex., Huppert and Turner, 1978, Huppert and Josberger, 1980) and field measurements (Horne, 1985) have shown the

presence of upwelling near the ice face as well as interleaving layers extending away. Near a glacier face (see Horne 1985), the buoyant meltwater creates an inner boundary layer, turbulent or laminar depending on the Grashof number, which rises. An outer downwelling layer (from 0.5 to 5 kms away from the ice face) was also observed. Meltwater mixes as it moves upward, entraining ambient fluid, until it reaches a density equal to that of the surrounding water and extends out as layers into the warmer, saltier water. As heat is lost preferentially to salt, the ambient fluid loses heat, increases in density and downwells. Double-diffusive exchanges cause the meltwater layers to rise as they move away from the wall. Upwelling velocity on the order of 1.7×10^{-3} m/s was calculated by Horne for one particular site with suggestions that it may be larger for icebergs in warmer water.

Wind-driven upwelling near coasts also gives rise to fronts. These are prograde fronts (i.e., frontal isopleth slopes are the same as the cross-shelf topography, Mooers et al., 1978). Shoreward of the front, the recently upwelled water is relatively dense compared to the surface water seaward of the front. Over seasonal time scales, such as off Oregon, the transport of water offshore creates a horizontal pressure gradient which in turn drives an along-shore surface current near the upwelling front over the shelf, and an opposite undercurrent near bottom over the upper slope region (see Mooers, et al., 1978). Transient events may be quite strong and perturb this seasonal picture. Wind-driven upwelling near fast-ice edges was discussed by Clarke (1978) and results from an "infinite" stress curl at the ice edge similar to coastal upwelling, due to the change in wind stress over ice and water. Pack-ice can also lead to upwelling along its edge, if the distance the pack ice moves perpendicularly to the ice edge, over the wind event, is small compared to the Rossby radius of deformation and if the change in ice density within the radius is sufficient to drop the wind stress to negligible values over the pack ice (Clarke 1978).

4.3 Longitudinal Mixing

Estimates of longitudinal mixing in the deep ocean have been reviewed by Garrett (1979). Dye studies by Okubo (1981), also resulted in estimates for the surface mixed layer. In both cases, K_h was of the order $10^2 - 10^3$ m^2 s^{-1}.

In estuarine waters, salt balance estimates can be used to calculate the effective horizontal dispersion coefficient. Holloway (1981) examined the upper reaches of the Bay of Fundy, a well-mixed estuarine system, and obtained an estimate of 300 m^2 s^{-1} (max. of 850 $m^2 s^{-1}$ in Minas channel) for K_h. The necessary variation in K_h to account for the observed salinity distribution, was found to be well described by the parametric equation 200 $\overline{u_* h}$ were u_* is the RMS friction tidal current velocity averaged over the M_2 tide, h is the water depth and the overbar indicates a cross-sectional average. Estimates for shear dispersion have the same functional form, however with the constant reduced to approximately 25 for the Bay of Fundy. Shear dispersion occurs when vertical mixing (parameterized as $K_v \sim .06\, u_* h$ for a well-mixed estuary - see Fisher et al., 1979), is interacting with a shear in the current and results in a spreading out of a tracer in the direction of flow. The influence of oscillating currents on K_h due to shear dispersion depends on the ratio of T/T_c where T is the period of the flow and T_c is the time required for mixing over the water depth. K_h is independent of T/T_c for $T/T_c \gg 1$. It is reduced for $T/T_c \ll 1$ and can be expressed as $K_h = (S^2 / \omega^2) K_v$ where S^2 is the mean-square vertical shear of the horizontal current which oscillates with frequency ω (see Garrett and Loder, 1981). For $T/T_c \gg 1$, K_h is proportional to $C\, u_* h$ with a value of C between 6 and 25 (Bowden, 1965). To account for the larger value of K_h obtained in the Bay of Fundy, Holloway suggested that a Zimmerman-type mixing mechanism may be occurring (see Zimmerman 1976, 1978). The basis of Zimmerman's approach lies in the superposition of Eulerian residual eddies and an oscillating tidal current. As tides move over changing bottom topography, non-linear interactions result in the formation of residual current eddies around the bottom perturbations. Assuming that these perturbations are more or less randomly distributed over the bottom, this results in a random distribution of eddies (in both strength and size). If an oscillating current is now superimposed on this field, a net Lagrangian dispersion of water parcels will result. Zimmerman parameterized the effective longitudinal dispersion as

$$K_h = b(\mathcal{Z}, \lambda) U_1 L_1$$

where U_1 is the tidal velocity, L_1 the tidal excursion and **b** is a function of the energy density spectrum of the residual current velocity field weighted by a function depending on γ (ratio of tidal/residual RMS velocity) and λ (ratio of tidal/residual length scales). For the Dutch Wadden Sea, Zimmerman obtained values for $K_h \sim 800$ m $^2s^{-1}$.

In stratified estuaries, a gravitational circulation is driven by the longitudinal density gradient, due to river influx, which can transport tracers up or down the estuary. A review of the parameterization of this process is given in Fisher et al. (1978) as well as the numerous limitations in field calculations.

Loder et al. (1982) made estimates of horizontal exchange across the flank of Georges Bank by examination of the evolution of temperature on top of the Bank with seasonal solar heating. K_h estimates ranged from 150 - 380 m^2s^{-1}. Estimates due to mixing by internal tides on the Scotian shelf had an upper bound of $K_h \sim 200$ m^2/s (Petrie, 1975).

4.4 Langmuir Circulation

Langmuir circulation will be classified as a mesoscale feature as it can be considered to consist of an "organized" cellular flow pattern in the surface mixed layer with set length and velocity characteristics. A good review of the form and dynamics of Langmuir cells is given by Leibovich (1983). The following summarizes salient features and is taken from this report.

Langmuir cells or "windrows" consist of parallel vortices with axes aligned with the wind direction (maximum deviation less than 20°), a range in spacing of meters to hundreds of meters, a length of 20 to 100 times the spacing (i.e., tens of meters to kilometes), and a penetration depth related to density stratification though generally having an aspect ratio (spacing/(2* depth)) close to 1. A threshold wind speed of 3 m/s is usually taken as the minimum wind speed required for cells to develop in a stable water column. Cell development and change in orientation under a wind direction shift occurs rapidly (i.e., minutes). There generally exist an hierarchy of windrows with both small scale temporary cells and relatively permanent large scale cells. The vortices are asymmetric and alternating in rotation leading to areas of convergence and divergence at the surface with positively buoyant particles swept along the surface to accumulate over areas of downwelling. The asymmetry is seen as intense downwelling, with speeds of the same order as the wind induced surface currents (.03 - .08 m/sec) contained in a narrow band with a broad, return upwelling over the rest of the cell (measured speeds less than half downwelling values). As a result of the circulation pattern, both positively and negatively buoyant particles may become trapped within a Langmuir cell depending on their relative terminal velocities. An analysis related to dispersed oil particles was performed by Leibovich and Lumley (1982) and that for bubbles by Thorpe (1984).

There are two independent sets of theories on the development of Langmuir circulation related to wave-current interactions. The model proposed by Garrett (1976), involves an amplification of waves in a region of increased horizontal current (such as observed in the long-wind surface current above the downwelling jet) which leads to preferential wave breaking - momentum transfer to the current as well as a surface convergence. This is a positive-feedback mechanism which eventually would lead to roll motions aligned in the wave propagation direction. A second set of theories, the Craik-Leibovich theories, are more generally accepted to describe the dynamics. These are related to fluctuations in vorticity, either through a direct drive (Theory I) or instability (Theory II) mechanism. In Theory I, the interaction between

the waves Stokes drift and a vorticity due to an existing current results in a "vortex force" which is normal to both the Stokes drift set up by the waves parallel to the wind and with the vorticity associated with the mean current shear with depth. The "vortex force" is obtained after averaging over time to obtain a rectified water motion. If the Stokes Drift varies across the wind direction in a coherent manner, the corresponding horizontal variation of the vortex force will result in a torque and overturning. In Theory II, the waves do not need to have any particular coherent distribution. Any small cross-current irregularity in the along-wind current would lead to vertical vorticity and a horizontal vortex force, when combined with the Stokes drift, directed towards the maximum of the current irregularity. This force leads to acceleration of the surface layer, sinking of fluid at the convergence zone and an increase in the amplitude of the current anomaly in the absence of friction (i.e., positive-feedback). For further discussion on these theories, see Leibovich (1983) and references cited therein.

5. MICROSCALE FEATURES

5.1 Vertical Mixing

There are primarily two groups of mechanisms leading to vertical mixing in the ocean: 1) interfacial shears and 2) buoyancy - convective mixing.

Interfacial shears result from a jump in velocity and density across an interface. Surface and bottom boundary layer mixing is the most obvious example. Shears in frontal zones were discussed in Section 4.2. A shear between two stably stratified fluids having different velocities can lead to the development of an instability (i.e., wavelike) which results in water overturn generating local turbulence. The fastest growing instability is of the Kelvin-Helmholtz (K-H) type, shown in experiments and theoretically by Miles (1961) to occur when the gradient Richardson number falls below 1/4. The range of wavelengths leading to this instability are on the order of 7.5 H to 6.3 H where **H** is the length scale of the interface thickness (see Turner, 1973). The maximum thickening of the interface (i.e. reduced density gradient) due to K - H instabilities is related to the balance between changes in kinetic and potential energy and given by $2\rho_o u^2/g\delta\rho$ with a typical value given by $0.3\rho_o u^2/g\delta\rho$ (see Turner, 1980). Once breaking occurs, the Richardson number increases above 1/4. An increase in the shear is required to again reduce the Richardson number and this can be supplied by the internal wave field in the ocean.

Buoyancy-convective mixing has already been discussed in terms of double-diffusive mechanisms at fronts in section 4.2. Other examples include mixing of the surface layer due to vernal cooling and salt extrusion (ice formation) and buoyancy flux of meltwater from an ice face (section 4.2).

When searching for evidence of turbulence, one must separate areas of active from fossil turbulence. In areas of active turbulence, energy is beng input to the system and further mixing or entrainment can occur. Fossil turbulence is a remnant signature of a previous mixing event (ex. breakng internal wave) and energy is no longer available for further mixing. Fossil turbulence results from the unequal dissipation of turbulent kinetic energy and the gradients of scalar properties which are usually measured. The persistence of a fossil patch increases with the parameter γ_o/N where γ_o is the rate of strain of turbulence at the time of fossilization ($= (\epsilon/\nu)^{1/2}$, ϵ = energy flux, ν = eddy viscosity) and **N** is the Brunt-Vaisala frequency (see Gibson, 1980). For active turbulence to be present the length scale, **L**,

of measured variations, must be smaller than the Osmidov scale, L_R (= $(\epsilon/N^3)^{1/2}$), where inertial forces of active turbulence equals the buoyancy force of local stratification and much greater than the Kolmogoroff scale, L_K (= $(\nu^3/\epsilon)^{1/4} = (\nu/\gamma)^{1/4}$) where viscous forces equal inertial forces (i.e., $L_R \gg L \gg L_K$). A third important length scale is the Batchelor scale, L_B (= $(D_C/\gamma)^{1/2}$ where D_C is the molecular diffusivity of a scalar c), representing the smallest feature in a turbulent scalar field (i.e., molecular diffusion balancing convection due to the turbulence) (see Gibson, 1980). For fossil turbulence, γ is replaced by N in both the expressions for L_K and L_B. If one considers dispersed oil droplets as a scalar, an equivalent scale to the Batchelor scale can be derived based on the dissolution rate of the droplet.

Following Gargett (1984), the change in concentration, c, per unit time, resulting from diffusion processes can be given as:

$$\frac{\partial c}{\partial t} = -u_i \frac{\partial c}{\partial x_i} - \overline{u_i' \frac{\partial c'}{\partial x_i}} + \frac{\partial}{\partial x_i}\left(D_c \frac{\partial c}{\partial x_i}\right) + F \qquad 5.1$$

where primes indicate variation from a mean, D_C is the molecular diffusivity, U_i the advective velocity, F source or sink terms and the overbar is some ensemble average. The second term in RHS of eq. 5.1 can be written as:

$$\overline{-u_i' \frac{\partial c'}{\partial x_i}} = \frac{\partial}{\partial x_i}\overline{(-u_i' c')} = \frac{\partial}{\partial x_i}\left(K_{ij} \frac{\partial \bar{c}}{\partial x_i}\right) \qquad 5.2$$

where K_{ij} is a parameterization of mixing by turbulent eddies, chosen to resemble the molecular diffusion formulation.

The RHS can be expanded, for the vertical component, to

$$\frac{\partial}{\partial z}\left(K_v \frac{\partial c}{\partial z}\right) = K_v \frac{\partial^2 c}{\partial z^2} + \frac{\partial K_v}{\partial z}\frac{\partial c}{\partial z} \qquad 5.3$$

Generally, as $K_{ij} \gg D_c$, the molecular diffusivity term is ignored, exceptions being in the analysis of double-diffusive fluxes and when the relevant length scales are such that diffusive subranges are important in turbulence studies. The second term in the RHS of eq. 5.3 is often set to zero assuming no depth dependence of K_v. However, if kept, this term provides a "pseudo-velocity" or advection of c. Gargett and Holloway (1984) have suggested that turbulence due to breaking internal waves should result in a parameterization of K_v as

$$k_v = \frac{R_f \epsilon N^{-2+p}}{1 - R_f} = a_o N^{-q} \qquad \begin{matrix} 1.0 \leq p \leq 1.5 \\ -1.0 \leq q \leq -0.5 \end{matrix}$$

where R_F is the flux Richardson number (~ 0.20). Both ϵ and a_o are site specific parameters.

For practical applications, various approximations may be used to estimate values of K_v. For homogeneous water columns, mixing resulting from bottom friction, Csanady (1976) suggests parameterizing K_v as

$$K_v = u_* H / 20 \quad \text{if} \quad H < 0.1\, u_* f$$

$$K_v = u_*^2 / 200f \quad \text{if} \quad H > 0.1\, u_* f$$

where u_* is a friction velocity equal to the square root of the drag coefficient ($C_d \sim 2.1 \times 10^{-3}$) times a depth averaged velocity (i.e., $C_d^{1/2}\, u$), **H** is the water depth and **f** is the Coriolis parameter. In the presence of stratification, K_v would be reduced by a function of the Richardson Number, such as $K_v = K_{v_o} (1 + 7\, R_i)^{-1/4}$ suggested by Bowden and Hamilton (1975). The constants for this expression are obtained through experimental fits and the expression is generally only applicable in shallow seas and well-mixed estuaries.

Estimates for K_v within the surface mixed layer span (i.e., two-layer systems) 3 orders of magnitude ($\sim .5 \times 10^{-4}$ - 10^{-2} m^2/sec^{-1}, Denman and Gargett (1983)). Under various assumptions, the scales of eddy motion in the surface mixed layer can be used to estimate K_v which can be applied in analytical or numerical models of oil dispersal in the mixed layer. The following development is extracted from Denman and Gargett (1983).

For a uniform stress layer (taken as the homogenous surface mixed layer), the important parameters are ϵ, W_*, the turbulent friction velocity (related to wind speed through the assumption of constant windstress across the air-sea interface

$$\tau = \rho_a C_{10} U_{10}^2 = \rho_a u_*^2 = \rho_\omega w_*^2$$

where ρ_a = air density, ρ_ω = water density, U_{10} = 10 meter wind speed, $C_{10} \sim 1.3 \times 10^{-3}$)) and N. Here, $\epsilon = w_*^3 / k_{vK} z$ where k_{vK} is von Karman's constant (0.4) and z is depth below the surface boundary. The largest eddy (vertical) that can exist in the surface mixed layer has a length scale equal to the Ekman depth, $L_e = 0.4\ W_* / f$, or the mixed layer depth, H, whichever is smaller. The time scale for movement around an eddy, T_m, is equal to L_m/U_T where U_T is the RMS eulerian velocity proportional to $2.0 * W_*$. For $L_m = L_e$, $T_m = 0.2/f$ implying a time scale independent of wind speed. For $L_m = H$, $T_m = L / U_T = L / 2 * W_*$ implying an inverse dependence on wind speed.

When stratification over a chosen distance becomes important, the length scale is determined by the buoyancy (Osmidov) scale, $L_R = (\epsilon / N^3)^{1/2}$. If the length scales of the largest eddies are less than the buoyancy scale, homogeneous turbulence can exist. At the surface, for water depths greater than $10 * L_R$, eddies scale as L_R, but for shallower depths, eddies feel the air-sea boundary and are controlled by surface stresses (i.e. $\epsilon = W_*^3 / (k_{vK} z)$). There is generally an order of magnitude difference between L_R in the surface mixed layer and in the thermocline.

When considering mixing, it is the Lagrangian motion that is important in order to determine the net displacement of a water parcel, or buoyant particle, with time. For example, detailed modelling of positions of dispersed oil particles requires knowledge of the Lagrangian displacement. Various approximations must be used to relate the Lagrangian field to the Eulerian measured components which is usually measured. These are also discussed by Denman and Gargett (1983). A Lagrangian integral time scale, T_L, is given by

$$T_L = \int_0^\infty R_L (T') \, dt'$$

where R_L (T') is the Lagrangian velocity auto-correlation function. For time scales less than T_L, $R_L \sim 1$ and the RMS vertical displacement of a particle can be obtained as

$$Z(t)^2 = U_T^2 T^2$$

where U_T is the Eulerian RMS velocity, as before, and T is time. For time scales greater than T_L,

$$Z(t)^2 = 2 U_T^2 T_L T$$

For large Reynold's number turbulence, $T_L \sim L_m / (3 U_T)$. Z(t) represents the standard deviation in the vertical of a Gaussian distribution. The expected position of a particle (or water parcel) at time T, compared to an initial position Z_o, is equal to $Z_o \pm Z(T)$ within certain confidence limits. When stratification becomes important,

$$K_v \sim U_T^2 T_L \qquad \text{or} \qquad Z(t)^2 = 2K_v T$$

(as long as Z(T) is less than initial depth of the particle).

On dimensional grounds, the energy flux, ϵ, can be related to K_v as

$$K_v \sim A \epsilon N^{-2}$$

where A is a constant around 0.25.

Oakey and Elliott (1982) have shown that in the surface mixed layer, the integral of ϵ over depth is proportional to the cube of the 10 meter wind speed. Hence K_v can be also estimated as

$$K_v \sim \frac{U_{10}^3}{H} N^{-2}$$

Direct estimates of K_v have been obtained using dye studies, tracers and direct measurements of property fluctuations from profiles. The approaches and limitations of these various methods are discussed by Gargett (1984). Of particular importance is the presence of the "pseudo-velocity" mentioned earlier, to tracer studies. Profiler methods assume a balance between K_v and the molecular diffusivity

of a scalar D_C as $K_v = CoD_C$. Co is a three-dimensional Cox number (if using temperature $= \left(\frac{\partial \overline{c'}}{\partial x}\right)^2 \Big/ \left(\frac{\partial c}{\partial z}\right)^2$). As the variance in only one dimension is usually measured, this expression is weighted by a factor of 1 to 3 depending on the degree of isotropy assumed. Gargett (1984) suggests a general inverse power law for K_v related to N (i.e., stratification) under all applications. This would greatly simplify modelling of vertical mixing processes.

The assumption of a uniform surface, constant stress layer for Lagrangian displacements, has been questioned due to the presence of turbulent patches associated with breaking waves and Langmuir circulation in the mixed layer (see Kitaigorodskii, 1984; Kitaigorodskii and Lumley, 1983; Kitaigorodskii et al., 1983; Thorpe, 1984). This is particularly important in oil dispersal studies as the physics involved in oil droplet formation is directly related to the level of turbulence (see Raj and Griffiths, 1979).

Kitaigorodskii (1984) suggested that the size of turbulent patches and characteristics of the turbulence related to breaking waves must reflect the energy balance in the equilibrium range of the surface gravity wave spectrum. He assumed that the energy flux, ϵ, goes entirely from low to high wavenumbers (however, there is some question of energy being transferred to lower wavenumbers as well) with all wave breaking occurring by a cut off wavenumber $k_g \sim 10^{-2} g / \epsilon^{2/3}$ (g is gravitational acceleration). The values for k_g and T_g ($\sim 10\epsilon^{1/3}/g$), the cut off period, can be found by equating ϵ to the rate of energy loss per unit surface area obtained via a statistical (or probability) argument for the mean energy loss per wave cycle due to breaking and the second moment of the frequency wave spectrum. Assuming the stationary existence of a turbulent patch, conservation of energy requires $\rho\epsilon / H_E = \rho \overline{\epsilon_v}$ where H_E is the vertical dimension of the turbulent patch and $\overline{\epsilon_v}$ is viscous dissipation inside the patch. For the continuous existence of turbulence, the time scale of the lifetime of the patch ($T_T = H_E / \epsilon^{1/3}$) must be greater than the characteristic time scale of breaking events. This implies, for continued existence, that $T_T/T_g > 1$ and an estimate for $H_E > 10\epsilon^{2/3}/g$. These time and length scales will be important in assessing the behaviour of dispersed oil in the surface mixed layer, entrained by wave breaking events.

In order to examine the turbulence spectra beneath breaking waves, one has to separate wave velocity components from turbulent components (see Kitaigorodskii and Lumley, 1983; Lumley and Terray, 1983). Lumley and Terray (1983) did this by assuming a wave velocity linearly related to wave height, independent of turbulence

which is, in turn, obtained by removing all signals coherent with wave height. The resulting turbulence spectrum showed enhancement about the central wave frequency with aliasing into its harmonics. The combined equations governing the interaction between waves and turbulence are given in Kitaigorodskii and Lumley (1983).

Raj and Griffiths (1979) examined the formation of oil droplets and their splitting under breaking and non-breaking wave states. They estimated a minimum sea state for non-breaking globule formation at a significant wave height of 3 meters (a possible range of 2-4.7 meters). Droplet splitting, under breaking waves, is related to the Weber number:

$$We = \frac{\text{surface tension force}}{\text{inertia force}} = \frac{\tau_d}{\rho_w v_d^2 d^2}$$

such that splitting continues until We $\geq$ 1. (τ_d = surface tension of the oil, d = drop diameter, ρ_w = water density, v_d = RMS velocity difference over distance d). The smallest droplet size is given at We = 1 at equilibrium. (Note: this implies active turbulence. Under conditions of fossil turbulence, droplet size will increase.) Milgram et al, 1978 (as quoted in Raj and Griffiths, 1979) have shown that $d_{min} \quad L_K$ and have related it to ocean wave spectrum:

$$d_{min} \simeq 0.12 \frac{\tau^{3/5} \omega^{2/5}}{\rho_w^{2/5} g^{4/5}}$$

(ω = modal wave frequency) with a suggested d_{min} of 50 microns.

For oil films thinner than this, a second expression is needed:

$$d_{min} \simeq 0.3 \frac{\tau^{2/5} \omega^{4/15} h^{1/3}}{\rho_w^{2/5} g^{8/15}}$$

(h = thicknes of the film)

The downward dispersion of oil droplets from breaking waves is believed to be due to the entrainment of oil droplets in the turbulent wake and not from direct impulse forces. Milgram et al (1978) (as quoted in Raj and Griffiths, 1979), showed that the maximum depth of penetration is given by:

$$Z_{max} = 0.32 \frac{\dot{M}}{\rho_w C_w W_t}$$

where $\dot{M}$ = rate of loss of wave momentum per unit crest length

C_w = wave phase speed

W_t = terminal velocity of a drop which penetrates to depth Z_{max}

($Z_{max} \uparrow W_t \downarrow \Rightarrow Z_{max} \uparrow d \downarrow$, direct impulse assumptions would imply a direct relationship, i.e. $Z_{max} \uparrow d \uparrow$). The major problem with this approach, however, is that it does not take into account any stratification of the water column, limiting penetration depth nor how the presence of oil alters the sea state.

Thorpe (1984, a, b, c) examined the distributions of bubbles below the surface, in the mixed layer, both analytically and numerically, and obtained estimates for $K_v \sim .004 - .02\ m^2\ s^{-1}$. Models of air bubble behaviour are important in relation to the dispersion of oil due to wave breaking as much of the physics would be similar and the joint distribution of air and oil "bubbles" may be important as the faster rising air bubbles can entrain water, thereby affecting surfacing rates of oil (see Naess, 1981). Thorpe's model assumes that the size of the bubble is small compared to the Kolmogorov Scale, that they are spheres and are sufficiently dispersed to prevent bubble-bubble interaction. Turbulence is simulated by displacements of the water surrounding a bubble through a distance, L, in a random direction Θ so that the equivalent bubble displacement is $L \sin \Theta$ horizontally and $L\cos\Theta - W_b \Delta T$ vertically where W_b is the buoyancy velocity, a function of the bubble character incorporating changes in radius, gas composition, etc. The output is a concentration and size distribution with depth. Thorpe (1984 b, c) suggests that Langmuir circulation cells could significantly change both of these properties as observed in sonar displays of bubble distribution (see Fig. 2 in Thorpe, 1984(c)). The relative dominance of Langmuir circulation on three-dimensional turbulence assumed in an initial wave breaking event will have to be determined.

5.2 Behaviour of Suspensions

The behaviour of a suspension is generally considered to have rheological properties determined by the interaction of the dispersed phase with the surrounding medium. If the dispersed phase consists of small particles ($\sim$ 0.1 to 10 microns in diameter) inertial and gravity effects are ignored. In most studies only dilute suspensions are considered (i.e., no interaction of particles) and the suspension can then be treated to an equivalent fluid with an effective viscosity increased by a function of the volume fraction of the dispersed phase. This result was first discussed by Einstein in 1905 who suggested the formula $\nu = \nu_0 (1 + 5/2\ \Phi_*)$ where ν_0 is the viscosity of the ambient fluid and Φ_* is the volume fraction of the particles (see Herczynski and Pienkowska (1980) for a review on statistical theory related to suspension dynamics). This basic formula has been modified in various ways to account for such things as the shape of particles and Brownian motion (ex.: if Brownian motion is strong enough to overcome the hydrodynamic effects, the formula for ν becomes $\nu = \nu_0 (1 + 2.5\ \Phi_* + 6.2\ \Phi_*^2)$ (Herczynski and Pienkowska, 1980)).

The basic approach to handling suspension behaviour is to set out the analytical governing equations for the microscopic behaviour of the particles and then perform some sort of averaging. As a result, many simplifications must be introduced. The modelling approach detailed in Drew (1983), however, is flexible enough to account for many of the more complicated interactions including mixtures of different size particles, particle deformation, breaking or agglomeration (see references cited in paper). The basic formulation does not appear to be limited to non-inertial effects. Discussion on deformation and drop breaking is given in Rallison (1984). The one question still to be addressed is the behaviour of non-dilute suspensions when particle interactions become important.

For larger particles (i.e., order 10^{-4} - 10^{-2} meters), the averaging used in suspension theory would not apply and individual particle behaviour modelling is required. The formulations needed would be almost identical to that used by Drew (1983), before averaging. Various approximations must be made to simplify the equations (for example see Leibovich and Lumley, 1982, discussion), with concurrent loss of generality. These are dictated by the problem being examined and the computational expense involved.

The formation of water-in-oil emulsions, or "chocolate-mousse", is commonly observed in oil spills. These emulsions are neither dilute nor composed of small particles. The emulsion should be treated as a whole with properties similar to that of pseudo-plastics.

6. IMPLICATIONS FOR THE BEHAVIOUR OF OIL SPILLS

Depending on the scale and resolution, the sophistication required for modelling of an oil spill can vary from order of magnitude estimates to sophisticated four-dimensional numerical models (x, y, z, t). With respect to the long-term dispersion of the dissolved fraction of oil, a water mass or tracer analysis may be sufficient. Modelling complexity generally tends to increase as one decreases the time and space resolution required. In order to properly follow both a surface slick and the subsurface dispersed fraction, a coupled surface and subsurface model should be used.

A good review of the state-of-the-art modelling of oil spills is given by Huang (1983). Very little work has been performed regarding subsurface oil behaviour. Two approaches in subsurface modelling have been taken. The first is the SEADOCK model (see Williams et al., 1975) where measured current velocities are applied directly and the second is the URI (University of Rhode Island) model (see Cornillon et al., 1979) which uses the three-dimensional mass transport equations. In the URI model, individual particles are injected into the water column which is divided into cells. Calculated concentration gradients, and advective velocities from a circulation model, provide the diffusive and advective transports between the cells.

Two-dimensional behaviour of the dispersed oil phase has been examined for specific applications such as the effect of Langmuir cells (Leibovich and Lumley, 1982), distribution after chemical dispersion (Mackay et al., 1982), concentration profiles for different particle sizes (or buoyancies) after wave breaking (Johansen, 1982, USCG sea-oil interaction studies) and the physics governing oil droplet behaviour (Raj and Griffiths, 1979). These types of studies, however, have not been integrated directly into large scale oil spill models though the URI model is capable of doing so to some extent.

The importance of numerical models lies in their ability to calculate the complex interations between the physical and chemical processes that are occurring.

The basic requirements for a model include:

- choice of grid sizes, boundary conditions and time step which allows sufficient resolution of the smallest physical process of interest while maintaining computational stability and efficiency.

- means of separating time and spatial dependence to allow for simplification (i.e., certain processes can be taken as constant in time or space through selected averaging procedures).

- sufficient detail of the wind, wave and current field as well as water column structure.

- representative expressions, or the use of submodels, for the various spill and physical oceanographic processes occurring.

The "idealistic" model formulation would:

- Treat the initial spilled oil volume as surface, subsurface dispersed and dissolved fractons. Further sophistication can be obtained by introducing the composition of each fraction (i.e., low molecular weight alkanes, high molecular weight alkanes, aromatics, etc.) and following the behaviour of each component. This would allow for the direct calculation of oil properties such as viscosity, interfacial tension, etc., which are dependent on composition.

- Use of a four-dimensional model (x, y, z, t) and a variable or "nested" grid system whereby resolution is increased in specific areas of interest. A second approach, as taken by the URI model (see Cornillon et al., 1979) involves a fixed or "Eulerian" grid system for which the current, wind and water properties are specified, and a translating "Lagrangian" grid, moving and expanding to include all oil particles and maintaining the same vertical resolution. This model follows oil droplet concentration in each grid cell.

The following equations describe the specific interrelationships and parameters of interest to oil spill modelling.

- Conservation of Mass (i.e., total change of oil volume per unit time over the model area equals zero).

i.e. $$\frac{\partial}{\partial t} \Sigma V_{SURF} + \frac{\partial}{\partial t} \Sigma V_{DISP} + \frac{\partial}{\partial t} \Sigma V_{DIS} + S_{INK} = 0$$

where

V_{surf} = surface oil volume (or concentration) in grid square i, j, k = 0 at some time $t = m \Delta t$ (Δt = time step, m = no. of time increments passed). The summation is performed over all grid squares.

V_{Disp} = dispersed oil volume in grid square i, j, k = 1, n at time $t = m \Delta t$

V_{Diss} = dissolved oil volume in grid square 1, j, k = 1,n at time $t = m \Delta t$

Sink: sum of all oil lost to the system due to evaporation, biodegradation, settling, etc., from $t = 0$ to $t = m \Delta t$.

- Mass transport equation for the three fractions:

Surface Spill
$$\frac{\partial V_{SURF}}{\partial t} = F_{in} + RS - C_1 E_w - E_{V_1} - Dis_1 - \underset{\sim}{u}_s \cdot \nabla V_{SURF} - SPR$$

Dispersed Oil
$$\frac{\partial V_{DISP}}{\partial t} = \sum S_p \cdot E_w - RS - Dis_2 - ABS - \underset{\sim}{u}_{ss} \cdot \nabla V_{DISP} + \underset{\sim}{D}_{ss} \cdot \nabla^2 V_{DISP}$$

Dissolved Oil $z=1$
$$\frac{\partial V_{DISS}}{\partial t} = Dis_1 + Dis_2 - E_{V_2} - \underset{\sim}{u}_{ss} \cdot \nabla V_{DISS} + \underset{\sim}{D}_{ss} \cdot \nabla^2 V_{DISS}$$

$z = 2, n$
$$\frac{\partial V_{DISS}}{\partial t} = Dis_2 - \underset{\sim}{u}_{ss} \cdot \nabla V_{DISS} + \underset{\sim}{D}_{ss} \cdot \nabla^2 V_{DISS}$$

where $V(\ )$ is a function of x, y, z and t

- zero advective or mixing flux through upper and lower boundaries
- grid z = 0 is the surface spill, water column divided into grid z = 1 to n

The expressions on the RHS range in complexity from empirical representations using experimental or observed relationships to complex sub-models.

F_{in} = rate of oil supply to the surface at the centre of the model grid. This can be taken as a continuous supply or as an instantaneous spill of volume V_{init}. The latter is simpler as one assumes the entire volume to have uniform characteristics at time t = 0. By treating the supply as continuous or composed of small "spillets", an "age" dependence has to be incorporated and a marker particle approach required. This latter approach may prove necessary as direct observations of surface spills indicate a discontinuous nature, with concentrations along windrows, breaking up due to wave action or varying thickness across the spill (thick lenses interspersed over a thin sheen) which would influence entrainment, evaporation, etc. (Raj & Griffith, 1979).

RS = resurfacing of dispersed oil from grid z = 1 or upward migration of dispersed oil particles. This is a function of the volume of dispersed oil, the droplet size spectrum and droplet density (i.e., buoyancy) in each cell. Time dependence and spatial dependence results from specifications of $C_1 \cdot E_n$ and $SP \cdot E_n$.

$C_1 \cdot En$ = rate of entrainment of surface oil into the dispersed phase. Time dependence is related to the "age" of surface oil (i.e., changes in viscosity, surface tension, etc.), the nature of the surface oil (ex. thick residue, or thin slick resulting from resurfaced oil), and environmental parameters such as wind speed. C_1 reflects a spatial and temporal probability associated with entrainment mechanisms such as wave breaking, in turn related to the wave spectrum.

$\sum Sp \cdot En$ = size spectral partitioning in grid z = 1, n of the entrained oil such that $\sum S_p$ = volume fraction of En in grid z. This can be treated as an instantaneous input from an event such as wave breaking or incorporate more elaborate mechanisms such as drop splitting (i.e., shift in the spectrum to smaller sizes) or drop coalescing. Various resurfacing, sinking and absorption or mixing processes

could then be related to the shape of the particle size spectrum. Droplet behaviour related to turbulence is discussed in Raj and Griffiths (1979).

Ev_1 = rate of evaporation (and other loss processes) of the surface oil . It is a function of time related to the time change in oil properties (composition, viscosity, thickness) and environmental parameters such as temperature and wind speed.

Dis = rate of dissolution of the surface oil - input into grid cell k = 1 (all j's and i's), also a function of time due to "age" of surface oil and environmental parameters such as water temperature, salinity and concentration gradient of the dissolved component, and boundary layer dynamics at the oil-water interface.

$\underset{\sim}{U_s} \cdot \nabla V_{Surf}$ = advective flux with U_s representing an horizontal velocity due to wind, surface water currents, surface waves, etc. This is drift due to winds and waves requires knowledge of the regional wind field. Surface and subsurface currents may require input using a detailed circulaton model incorporating such things as tides, wind forcing, bathymetric effects, density structure, etc. Small scale processes could also be included such as Langmuir cells and frontal circulation.

SPR = rate of spreading of the surface slick due to gravity, surface tension and horizontal mixing. This is a time dependent process as the spreading mechanism and rate change with the evolution in spill size, thickness and chemical properties. The spreading of the surface spill indirectly controls the entrainment, evaporation (and other losses) and dissolution rates.

DIS_2 = rate of dissolution of the dispersed oil. It is a function of time due to droplet composition, the particle size distribution in the grid cell and local boundary layer dynamics controlling component solubility.

ABS = rate of loss due to absorption onto sediments, flocculation, ingestion by organisms, etc. and is a function of the droplet size and chemical properties.

EV_2 = rate of evaporative loss of the dissolved fraction to the atmosphere. It is a function of environmental parameters and presence or absence of surface oil which can act as a "ceiling".

$\underset{\sim}{U}_{SS} \cdot \nabla V_{Disp}$,
$\underset{\sim}{U}_{SS} \cdot \nabla V_{Diss}$ = advective transport. The vertical component, if desired, may incorporate the upward, buoyancy related, transport of the dispersed phase.

$\underset{\sim}{D}_{SS} \cdot \nabla^2 V_{Disp}$,
$\underset{\sim}{D}_{SS} \cdot \nabla^2 V_{Diss}$ = horizontal and vertical mixing of dispersed or dissolved oil. D_{SS} may be a function of horizontal position due to changes in water column structure (i.e., increased or decreased mixing), vertical position (ex: surface mixed layer vs pycnocline), time (ex: sporadic increase in mixing due to breaking internal waves and tides) and the physical nature of the oil (oil-in-water, water-in-oil emulsion or dissolved).

In general, the model should have enough flexibility to handle different oil types, additions of chemical dispersants and the formation and subsequent behaviour of water-in-oil emulsions. The model as described above would be extremely complex if all the suggested interactions are incorporated. Various assumptions, averaging or submodels can be used to simplify or ignore some of the processes. One of the most difficult processes to account for and one of the most important due to the effective increase in oil density which could lead to sinking, is the formation of water-in-oil emulsions or "chocolate mousse". The formation tendency will be dependent on the chemical properties of the oil, in response to energy input to the slick. The stability of the emulsion will reflect, again, viscosity, composition of the oil and the size distribution of the encompassed water drop (see Mackay and Zagorski, 1982). The model may include a sub-model branch used when threshold mixing and oil properties are such that emulsion formation is expected. Within this submodel, emulsion separation, break-up into "packets" due to mixing, altered relationships with dissolved and dispersed fractions, etc., would be taken into account. The physical behaviour of

the emulsion is more like a pseudoplastic than a Newtonian fluid and the rheological properties will thus differ from those of an equivalent water mass. The necessary governing equations and parameters would be determined through experimental observations. Unfortunately, most experiments cannot reproduce actual environmental conditions and those examining rheological properties of two-phase flows have concentrated on dilute suspensions.

The first step in model simplification is to separate the various processes into time (or spatial) varying and non-varying components through a scaling argument. To do this, ideally one should formulate all the chemical processes (i.e., evaporation, dissolution, emulsion formation) as a function only of time, initial oil composition or type and environmental parameters (i.e., wind speed, temperature). Oil "aging" would be incorporated in this time function through bulk parametric relationships related to initial oil type or to viscosity, density or interfacial tension detailed from lab experiments or field observations. The existing uncertainties in the chemical behaviour of the spill as well as the often poor wind and physical oceanographic data base may not warrant incorporation of highly complex expressions in the large scale model. The chosen model grid size and time step will determine those processes which can be detailed and those which must be parameterized due to the necessary assumption of uniform properties within a spatial grid and constant behaviour over a time step. The model scales provide a lower limit while the length of the model run, in essence, determines an upper limit. For processes varying on time scales longer than the model run, they may be represented as a constant mean or extreme behaviour.

The choice in grid scales, time steps and length of run is dependent on both the site and spill characteristics. The initial spill volume (and area) will set the upper limit on horizontal grid size. The length of run can be determined by such things as model boundaries or percentage of oil volume remaining in the study area. The lower limits (i.e., highest resolution) is by choice of the modeller though certain physical or chemical characteristics may set lower bounds.

When examining the dispersed fraction of oil and choosing between depth-averaging (or time-averaging) the surface mixed layer or resolving it directly, the relative time scales for resurfacing, entrainment and dissolution of the dispersed oil may determine the approach needed. The following illustrate the possible interactions between these three processes.

Let RS_t: resurfacing time scale - function of particle buoyancy and vertical mixing (K_v)

En_t: entrainment time scale - function of wave breaking

Dis_t: dissolution time scale - function of particle solubility and boundary layer dynamics

ii $RS_t \backsim En_t$ = steady-state volume and size spectrum in space though evolving in time

$RS_t > En_t$ = volume of dispersed fraction decreases over time step - entrainment may become negligible if $RS_t \gg En_t$

$RS_t < En_t$ = volume of dispersed fraction increases over time step - evolving spectrum in space

$RS_t \ll Dis_t$ = Can ignore RS contribution to surface slick

$En_t \ll Dis_t$ = Can ignore dispersed oil fraction in the water column

$RS_t \gg Dis_t$ = Can ignore dissolution of dispersed particles

The important time scales, in order to determine the above relationships, range from ~15 minutes to ~1 day depending on the particle size (or buoyancy) and mixing rate (assume terminal velocity between .001 - .01 m/s and $K_v \backsim 10^{-2}$ m^2/sec). The corresponding length scales are on the order of meters. Entrainment rates, can be related to wave breaking events which have time scales on the order of the wave period (i.e. seconds) during storms and length scales related to wave height (i.e., meters). Langmuir cells may effectively increase the retention of droplets. These are the smallest scales that can be resolved, however using time scales on the order of seconds or minutes is often impractical. Other necessary model inputs, such as the wind field, generally have time resolutions longer than this (ex. three hours) by which point some sort of "average" concentration and size spectral profile would have been established. Some model parameters, such as a longitudinal tidal dispersion coefficient, have an implicit time - average application. Averaging in time or space simplifies the model and may provide sufficient resolution for large scale trajectory models. However the surface spill should always be treated separately though coupled to the subsurface fraction due to differing governing equations.

The following summarizes the major physical characteristics of selected geographic areas along Canada's coast which should be taken into account when designing the appropriate oil spill model. Super-imposed on these are the small scale turbulence structures discussed in section 5. as well as ubiquitous features such as Langmuir cells, interfacial waves and surface gravity waves.

Newfoundland's Grand Banks

Major features:

- current system dominated by wind forcing on top of the Bank and by the presence of the two branches of the Labrador current
- the "tail of the Bank" is subject to large, periodic (order of months) perturbations due to the impingement of Gulf Stream meanders
- the water column consists of two-layers in the summer but uniformly mixed to the bottom in the winter
- subject to severe wave conditions
- intermittent presence of icebergs and pack-ice

The current regime varies on tidal (mixed), inertial (16 hours), synoptic (2-10 days) and seasonal (months, freshwater pulse) time scales. Given an oil spill at 47°N, 48°W, advective transport across one dimension of the Bank (600 kms) can occur in as little as 11 days (.6 m/s flow in the subsurface core of offshore branch of the Labrador current) or longer than 75 days (.1 m/s flow on top of the Bank). The shelf/slope break is approximately 100 kms wide and it is here that upwelling, internal waves and other mixing mechanisms are occurring with lengths scales on the order of 1-10 kms. As the water column is two-layer in the summer, a depth dependent model should be used. This density structure acts to decouple the surface and bottom layer from wind forcing so that the inertial signal is reduced at depth. Mixing across the pycnocline can be related to the density structure either parametrically through inverse dependence on the Brunt-Vaisala frequency or using the Richardson number. In the winter, the water column has a uniform density (26-27

σ_t) and will be responding, as a whole, to wind forcing with any depth dependence reflecting bottom friction effects. In the winter, the wave climate can be quite severe with significant wave height exceedances on the order of 30-40% greater than 4.0 m, 7-10% greater than 6.0 m and 1% greater than 9.0 m (Neu, 1982). Peak periods most frequently occur in the range of 8-12 seconds. The intermittent presence of icebergs may provide areas of intense mixing (10-100's meters) as described in section 4.2. The presence of pack ice may act as a barrier to pool surface oil while subsurface oil may extend below the ice sheet.

Gulf of St. Lawrence

Major features:

- current regime estuarine driven in the upper estuary, central and southeast Gulf and meteorologically driven in the northeast Gulf and Strait of Belle Isle, and to some extent through, Cabot Strait

- the estuary changes from "well mixed" to "stratified" near Gaspe peninsula showing opposite flow patterns with depth and across the width of the mouth. Opposite flow patterns can also be seen in Cabot Strait and the Strait of Belle Isle

- within the Gulf, the water column shows three layers in summer (in temperature and salinity) and two in winter and is subject to internal wave oscillations

- freeze-up begins in January, with no open water through March, break-up in late April with the possible exception in the northeast Gulf (slightly later).

The current regime varies on tidal (semi-diurnal), synoptic and seasonal time scales. The latter is dominant reflecting changes in St. Lawrence river runoff. This is also true for water column structure which is also responding to seasonal heating patterns (including ice formation and melt). Like most tidal estuaries, any pollutant released tends to be mixed along the length of the estuary. In the lower St. Lawrence, the presence of large eddies, can act to trap oil spilled in this region. At the peak of flow in May, surface oil present in the estuary (Gaspe current) will travel

down through Cabot Strait by August (~ 90 days). However any oil mixed below the surface layer (i.e. into the counter-current) will be retarded. The minimum flow occurs in March, a factor of 3 times less than May values. Flushing time of fresh water, is estimated around 6-8 months.

Scotian Shelf

Major features:

- current system characterized by a slow, residual flow along the shelf (east to west), upon which is superimposed meteorological and deep-ocean forcing (i.e. Gulf Stream rings)

- a thermo-haline front, as indicated by strong interleaving of shelf and slope waters, at the shelf/slope break which is subject to periodic perturbations (~ month) due to passage of warm-core rings in the slope waters

- the water column consists generally of two-layers in the summer, with a third deep layer in troughs. In the winter, the water column is uniformly mixed over banks, with slight stratification in the troughs.

The current regime varies primarily on tidal, synoptic, non-synoptic or deep-ocean forcing (10-90 days), and seasonal time scales (due to freshwater input from Cabot Strait). It takes approximately 4 to 5 months for a water parcel to travel the length of the Scotian Shelf. A particular feature of the Scotian Shelf is the bathymetric complexity with numerous banks and troughs. Proper modelling of the area would require resolution of these features as they affect circulation patterns, and the degree of vertical mixing in the water column.

The shelf/slope front will have particular importance when modelling the dispersed oil fraction as this is an area of increased horizontal exchange. The length scales of the interleaving layers (order 10^3 - 2 X 10^4 m), their thickness (10-20 meters) and mixing boundaries (.01 - 1 m) are sufficiently large for dispersed oil droplets, less than .01 m in diameter to be modelled by an approximate eddy diffusivity. The behaviour of water-in-oil emulsions, however, would be considerably different. Mixing at thermo-haline fronts is primarily diffusive, hence there is little energy to "break up" on emulsion showing some visco-elastic properties. The

emulsion would travel along the front, along isopycnals, or away from the front under "calving" processes or entrainment by Gulf Stream rings. As the ambient water surrounding the emulsion would have temperature and salinity characteristics different from the encapsulated water some manner of exchange may occur which could lighten the emulsion. The emulsion may act to dampen waves, with length scales less than that of the emulsion. The primary mixing mechanism capable of breaking up such a layer would be turbulence generated from breaking internal waves.

As 5 to 8 warm core Gulf Stream rings are formed per year, with generally 2 to 3 present in the slope waters from the tail of the Grand Banks to Cape Hatteras at any one time, it is conceivable that an oil spill occuring on the Scotian Shelf, particularly near the Shelf break, will be influenced by the passage of a ring. As rings entrain water from the shelf, a portion of the spill may be lost in this way. A spill occuring within a ring, is partially isolated from the surrounding waters and will translate down the coast at a rate of approximately 0.5 m/s. Exchange processes may result in some dispersed oil being left in the rings "wake".

Bay of Fundy - Gulf of Maine

Major features:

- current system dominated by tidal forcing and tidally generated residual currents with some estuarine driven flow in the Bay of Fundy and superimposed wind forcing

- water column structure reflects seasonal heating variously disrupted by tidal mixing

- important interactions between bathymetry and tides result in current gyres around banks (George's, Brown's) and shallow-sea fronts.

The current regime varies primarily on tidal scales though with some meteorological and seasonal (e.g. flow into the Gulf of Maine related to freshwater pulse which has travelled down the Scotian Shelf) forcing. Much of the residual circulation is tidally induced.

The presence of gyres, areas of upwelling, fronts, large values for longitudinal dispersion are all directly related to the tides and have implications to

oil spill behaviour. The two banks that have been studied, George's Bank and Brown's Bank, show current gyres around the edges and vertically well mixed water on top. The trajectory of a spill (surface and subsurface fractions) will reflect both this gyre influence and wind forcing (at the surface). At the edge of George's Bank, two modes of horizontal mixing have been identified, bottom upwelling and mid-depth internal tide breaking, both having implications to the subsurface oil dispersal. The depth dependence reflects the necessity for a model which resolves the water column structure, not only here but wherever shallow-sea fronts are found.

The large dispersion coefficients observed for the Bay of Fundy implies a very rapid spread of both the surface and subsurface oil fractions in this area. For clean-up purposes, this forces a rapid response to any accidental spill. The high sediment loads would also have to be taken into account due to the possible contribution to oil settling on the bottom.

Southeastern Beaufort Sea Shelf

Major features:

- current system dominated by the Mackenzie River, winds and density driven flow
- presence of ice through most of the year
- possible thermo-haline front at the shelf/slope break
- water column structure reflecting freshwater input from the Mackenzie River and ice melt or formation.

The current regime varies on tidal and inertial (both having approximately 12 hour periods), synoptic and seasonal time scales. Understanding of both estuarine and plume dynamics is necessary for modelling any oil spilled in this area. This includes eddy formation at the edge of the plume, which would disperse oil horizontally, and entrainment into the ambient water. The freshwater input acts to uncouple the surface and deep layer to wind forcing. Thermo-haline mixing processes, similar to those on the Scotian Shelf/slope break, could act to supply dispersed oil to deeper waters. Sediments carried by the Mackenzie River may act to leach oil out of the water column at one location and possibly resuspend them at another. This will be

particularly important within the 30 m isobath where the plume is concentrated. As arctic ecosystems are extremely sensitive to perturbations, very detailed modelling may be required in this location to assess potential spill damage.

7. CONCLUSIONS AND SUGGESTIONS FOR FUTURE WORK

This report summarizes the various physical oceanographic features, occurring in Canada's Atlantic and Beaufort Sea waters, which may influence the subsurface movement of oil. Both observational and theoretical studies have been made of many of these features, however the governing physics and proper parameterization of the processes often need to be better understood for practical applications and modelling. In many areas, the spatial and temporal coverage of direct observations is insufficient for proper calibration of transport models. In light of potential oil spill behaviour, further physical oceanographic studies should be concentrated around sensitive areas. Large scale models are useful in delineating these areas. Smaller scale, higher resolution models prove more useful for examination of clean-up procedures due to their ability of resolving areas of increased oil concentration (ex., fronts, Langmuir cells) or dispersal. Future efforts should also be directed in improving the parameterization of each constituent. There have been very few studies on the subsurface behaviour of oil and those related to dispersal in the surface mixed layer have not been extended to larger scale models nor integrated with other, simultaneously occurring, processes.

Laboratory experiments have been the major source of information on the chemical behaviour of spilled oil. Unfortunately, these suffer from being in an artificial environment and from having the necessary limitations imposed on the number of free parameters. The results are parameterized for model use but they often assume a linear superposition of processes. Future studies should be geared to account for various feedback processes and synergistic effects and performed in an environment as realistic as possible. The experimental design should take into account the physical scale implicit in the experiment and the results described in terms of the scales for practical application. Ideally, the chemical interactions should be reduced to a functional dependence only on the environmental parameters (i.e., temperature, mixing, wind speed, etc.) and time (i.e., "aging") to allow for integration into transport models. The current level of uncertainty in both the physical and chemical parameters does not warrant higher sophistication.

Some effort should also be made to couple oil spill models to those of suspended sediment transport, bubble injection at the surface, etc., whose components will be interacting with both the surface and dispersed oil fractions. In

many models, the presence of the oil has been assumed to have a negligible effect on the physical oceanography. The validity of this assumption should be tested with particular reference to wave breaking, details on fine and microstructure and the rheological properties of water-in-oil emulsions.

8. REFERENCES

Armi, L. 1978. Some evidence for boundary mixing in the deep ocean. J. Geophys. Res. 83: 1971-1979.

Baines, P.G. 1974. The generation of internal tides over steep continental slopes. Phil. Trans. Roy. Soc. London, 227, 1263: 27-58.

Benoit, J., M.I. El-Sabh, and C.L. Tang. 1985. Structure and Seasonal Characteristics of the Gaspe Current. J. Geophys. Res. 90: 3225-3236.

Bigelow, H.B. 1927. Physical oceanography of the Gulf of Maine. U.S. Dept. Comm. Bur. Fish. Bull. 40, 511 - 1027.

Bowden, K.F. and P. Hamilton. 1975. Some experiments with a numerical model of circulation and mixing in a tidal estuary. Est. Coastal Mar. Sci. 3:281-301.

Bowman, M.J. and R.L. Iverson. 1978. Estuarine and plume fronts. In: "Oceanic fronts in coastal processes". Ed. by M.J. Bowman and W.E. Esaias. Springer-Verlag. p. 87-104.

Butman, B., R.C. Beardsley, B. Magnell, D. Frye, J.A. Vermersch, R. Schlitz, R. Limeburner, W.R. Wright and M.A. Noble. 1982. Recent observations of mean circulation on Georges Bank. J. Phys. Ocean. 12, 569-591.

Clarke, A.J. 1978. On wind-driven quasi-geostrophic water movements near fast-ice edges. Deep Sea Res. 25:41-51.

Cornillon, P.C., M.L. Spaulding and K. Hansen. 1979. Oil Spill Treatment Strategy Modelling for Georges Bank. 1979 Oil Spill Conference Proceedings. pp. 685-692.

Csanady, G.T. 1976. Mean circulation in shallow seas. J. Geophys. Res. 81: 5389-5399.

de La Ronde, M. 1972. Temperature, salinity, and density distributions of the Scotian Shelf 1965 - 1971. Bedford Inst. of oceanography. Data Series. BI-D-72-6. 51 pp.

Denman, K.L. and A.E. Gargett. 1983. Time and space scales of vertical mixing and advection of phytoplankton in the upper ocean. Limnol. and Ocean. 28(5) 801 - 815.

Drew, D.A. 1983. Mathematical modelling of two-phase flow. Ann. Rev. Fluid Mech. 15:261-291.

Drinkwater, K., B. Petrie., W.H. Sutcliffe. 1979. Seasonal geostrophic volume transports along the Scotian Shelf. Est. Coastal Mar. Sci. 9, 17-27.

El-Sabh, M.I. 1975. Transport and Currents in the Gulf of St. Lawrence. Bedford Inst. of Ocean. Report Series BI-R-75-9. 180 pp.

El-Sabh, M.I. 1984. Physical Oceanography of the St. Lawrence Estuary. 1984. CMOS Conference (abstract only).

Farquarson, W.I. and W.B. Bailey. 1966. Oceanographic Study of Belle Isle Strait 1963. Bedford Inst. of Ocean. Report 66-9. 78 pp.

Fisher, H.B., E.J. List, B. Koh, J. Imberger and N.H. Brooks. Mixing in Inland and Coastal Waters. Academic Press. N.Y. 1979. 438 pp.

Fissel, D.B. 1981. An analysis of current meter data obtained at CANMAR Drillships 1976-1979. Prep. by Arctic Sciences Ltd. for Dome Petroleum Ltd. 126 pp.

Fissel, D.B. and J. R. Birch. 1984. Sediment transport in the Canadian Beaufort Sea. Prep. for Atl. Geoscience Centre, Bedford Inst. of Ocean., Dartmouth Nova Scotia, 165 pp. (unpub. man.).

Gargett, A.E. 1984. Vertical eddy diffusivity in the ocean interior. J. Mar. Res. 42: 359-393.

Gargett, A.E. and G. Holloway. 1984. Dissipation and diffusion by internal wave breaking. J. Mar. Res. 42: 15-27.

Garrett, C.J.R. 1976. Generation of Langmuir Circulation by surface waves -a feedback mechanism. J. Mar. Res. 34:117-130.

Garrett, C.J.R. 1979. Mixing in the ocean interior. Dyn. of Atm. and Oceans. 3, 239-265.

Garrett, C.J.R. and E. Horne. 1978. Frontal circulation due to cabbeling and double diffusion. J. Geophys. Res. 83: 4651: 4656.

Garrett, C.J.R., J.R. Keeley and D.A. Greenberg. 1978. Tidal mixing vesus thermal stratification in the Bay of Fundy and Gulf of Maine. Atm-Ocean 16 (4) 403 - 423.

Garrett, C.J.R. and J.W. Loder. 1981. Dynamical aspects of shallow sea fronts. Phil. Trans. Roy. Soc. Lond. A. 302: 563-581.

Garrett, C.J.R. and R.H. Loucks. 1976. Upwelling along the Yarmouth Shore of Nova Scotia. J. Fish. Res. Bd. of Can. 33, 116-117.

Garrett, C.J.R. and W. Munk. 1972. Space-time scales of Internal waves. Geophys. Fluid Dyn, 2, 225-264.

Garrett, C.J.R. and W. Munk. 1975. Space-time scales of internal waves: a progress report. J. Geophys. Res. 80:291-297.

Garrett, C.J.R. and B. Petrie. 1981. Dynamical aspects of the flow through the Strait of Belle Isle. J. Phys. Ocean. 11, 376-393.

Garrett, C.J.R. and B. Toulany. 1981. Variability of the flow through the Strait of Belle Isle. J. Mar. Res. 39, 163-189.

Garrett, C.J.R. and B. Toulany. 1982. Sea Level variability due to meteorological forcing in the Northeast Gulf of St. Lawrence. J. Geophys. Res. 87: 1968 - 1978.

Garvine, R.W. 1980. The circulation and thermodynamics of upper ocean density fronts. J. Phys. Ocean. 10: 2058-2081.

Gatien, M.G. 1976. A study in the slope water region south of Halifax. J. Fish. Res. Bd. Can. 33: 2213 - 2217.

Gibson, C.H. 1980. Fossil Temperature, Salinity and Vorticity Turbulence in the Ocean. In: "Marine Turbulence". Ed. by J.C.J. Nihoul. Elsevier Oceanographic Series No. 28. Proc. of the 11th. Inter. Liege Colloq. on ocean Hydrodynamics. p. 221-257.

Gill, A.E. Atmosphere - Ocean Dynamics. 1982. Academic Press, N.Y. 662 pp.

Gill, A.E. and A.J. Clarke. 1974. Wind-induced upwelling, coastal currents and sea level changes. Deep-Sea Res., 21, 325 - 345.

Greenberg, D.A. 1983. Modelling the mean barotropic circulation in the Bay of Fundy and Gulf of Maine. J. Phys. Ocean 13: 886-904.

Herczynski, R. and I. Pienkowska. 1980. Toward a statistical theory of suspension. Ann. Rev. Fluid Mech. 12: 237-269.

Holloway, G. 1983. A conjecture relating oceanic internal waves and small-scale processes. Atm-Ocean, 21(1):107-122.

Holloway, P.E. 1981. Longitudinal mixing in the upper reaches of the Bay of Fundy. Est. Coastal and Shelf Sci. 13, 495 - 515.

Hopkins, T.S. and N. Garfield. 1979. Gulf of Maine intermediate water. J. Mar. Res. 37, 103-139.

Horne, E.P.W. 1978. Physical aspects of the Nova Scotian Shelf Break Front. In: "Ocean Fronts in Coastal Processes" Ed. by M.J. Bowman and W.E. Esaais. Spring-Verlag. P59-68.

Horne, E.P.W. 1985. Ice-induced vertical circulation in an Arctic Fiord. J. Geophys. Res. 90: 1078-1086.

Horne, E.P.W., M.J. Bowman and A. Okubo. 1978. Cross frontal mixing and cabbeling. In: "Oceanic fronts in coastal processes." Ed. by. M.J. Bowman and W.E. Essias. Springer-Verlag. p. 105: 113.

Huang, J.C. 1983. A review of the state-of-the-art of oil spill fate/behaviour models. 1983 Oil Spill Conference Proceedings. pp. 313-322.

Huntsman, A.G., W.B. Bailey and H.B. Hackey. 1954. The general oceanography of the Strait of Belle Isle. J. Fish. Res. Bd. of Can. 11, 198-260.

Huppert, H.E. and E.G. Josberger. 1980. The melting of ice in cold stratified water. J. Phys. Ocean. 10: 953-960.

Huppert, H.E. and J.S. Turner. 1978. On melting icebergs. Nature 271: 46-48.

Isaji, T. and M.J. Spaulding. 1984. A model of the tidally induced residual circulation in the Gulf of Maine and Georges Bank. J. Phys. Ocean. 14/6: 1119-1126.

Johansen, O. 1982. Dispersion of oil from drifting slicks. Spill Tech. Newsletter. pp. 134-158.

Juszko, B.A. 1981. The Strait of Belle Isle - Physical Aspects and Biological Implications of the Flow. M.Sc. Thesis. Dalhousie Univ., Halifax, N.S. 152 pp.

Juszko, B.A., D.R. Green and J.R. Birch. 1983. A study of the oceanographic conditions suitable for the sinking of oil. A report prepared for the Env. Protection Service. Dept. of the Environment. 181 pp.

Keeley, J.R. 1981. Mean conditions of potential temperature and salinity along the Flemish Cap section. Mar. Env. Data Service Technical Report No. 3. 45 pp.

Khandekar, M.L. 1980. Inertial oscillations in floe motions over the Beaufort Sea - Observations and Analysis. Atm - Ocean. 18, 1-14.

Kitaigorodskii, S.A. 1984. On the fluid dynamical theory of turbulent gas transfer across an air-sea interface in the presence of breaking wind waves. J. Phys. Ocean. 14: 960-972.

Kitaigorodskii, S.A., M.A. Donelan, J.L. Lumley and E.A. Terray. 1983. Wave-turbulence interaction in the upper ocean. Part II: Statistical Characteristics of Wave and Turbulent Components of the Random Velocity Field in the Marine Surface Layer. J. Phys. Ocean. 13:1988-1999.

Kitaigorodskii, S.A. and J.L. Lumley. 1983. Wave-Turbulence Interactions in the Upper Ocean. Part I: The Energy Balance of the Intracting Fields of Surface Wind Waves and Wind-Induced Three-Dimensional Turbulence. J. Phys. Ocean. 13:1977-1987.

Lai, D.Y. and P.L. Richardson. 1977. Distribution and movement of Gulf Stream rings. J. Phys. Ocean 7, 670 - 683.

Lauzier, L.M. 1967. Bottom residual drift in the continental shelf area of the Canadian Atlantic Coast. J. Fish. Res. Bd. Can. 24, 1845-1858.

Leibovich, S. 1983. The form and dynamics of Langmuir Circulations. Ann. Rev. Fluid Mech. 15: 391-427.

Leibovich, S. and J.L. Lumley. 1982. Interaction of turbulence and Langmuir cells in vertical transport of oil droplets. In "Proc. of the First Int. Conference on meteorology and air-sea interaction of the coastal zone". The Hague, Netherlands.

Loder, J.W. 1980. Topographic rectification of tidal currents on the sides of Georges Bank. J. Phys. ocean. 10: 1399-1416.

Loder, J.W. and D.G. Wright. 1985. Tidal rectification and frontal circulation on the sides of Georges Bank. Subm. to J. Mar. Res.

Loder, J.W., D.G. Wright, C. Garrett and B.A. Juszko. 1982. Horizontal Exchange on Central Georges Bank. C.J. Fish. and Aquat. Sci. 39(8), 1130: 1137.

Louis J.P., B.D. Petrie and P.C. Smith. 1982. Observations of topographic Rossby waves on the continental margin off Nova Scotia. J. Phys. Ocean. 12, 47-55.

Louis, J.P. and P.C. Smith. 1982. The development of the barotropic radiation field of an eddy over a slope. J. Phys. Ocean. 12: 56-73.

Magaard, L. and W.D. McKee. 1973. Semi-diurnal tidal currents at site 'D'. Deep Sea Res. 20: 999 - 1009.

Mackay, D., S. Chang and P.G. Wells. 1982. Calculation of oil concentrations under chemically dispersed slicks. Mar. Poll. Bull. 13/8: 278-283.

Markham, W.E. 1975. Ice climatology in the Beaufort Sea. Beaufort Sea. Techn. Report No. 26. Beaufort Sea Project. 87 pp.

Marsden, R.F. 1985. The internal tides on Georges Bank. Submitted to J. Mar. Res.

Matthews, J. 1976. Oceanography of the Labrador Coast - A Review. Unpub. manuscript.

McLellan, H.J. 1957. On the destinations and origins of the slope waters off the Scotian Shelf and its easterly flow south of the Grand Banks. J. Fish. Res. Bd. Can. 14: 213-239.

Melling, H. 1983. Oceanographic features of the Beaufort Sea in early winter. Can. Tech. Rep. Hydrogr. Ocean Sci. 5: 131 pp.

Miles, J.W. 1961. On the stability of heterogeneous shear flows. J. Fl. Mech. 10: 496-508.

Mooers, C.N.K. 1975. Several effects of a baroclinic current on the cross-stream propagation of vertical internal waves. Geophys. Fl. Dyn. 6:245-275.

Mooers, C.N.K., C.N. Flagg and W.C. Boicourt. 1978. Prograde and Retrograde Fronts. In: "Oceanic fronts in coastal processes". Ed. by M.J. Bowman and W.E. Esaias. Springer-Verlag. p. 43:58.

Naess, A. 1981. On the residence time of oil mixed into the water column by breaking waves. Offshore Tech. Conf. Proceedings Vol II, May 4-7. Houston, Texas. Paper No. 4064. pp. 497-508.

Neu, H. 1982. 11-year Deep Water Wave Climate of Canadian Atlantic Waters. Can. Tech. Rep. Hydrogr. Ocean. Sci. 13: 7, 41 pp.

Nihoul, J.C.J. 1980. The Turbulent Ocean. In: "Marine Turbulence. Proc. of the 11th Int. Leige Colloquim in Ocean Hydrodynamics". J.C. Nihoul ed. Elsevier Oceanographic Sciences. No. 28 p. 1-20.

Okubo, A. 1971. Oceanic diffusion diagrams. Deep Sea Res. 18: 789-802.

Petrie, B.D. 1975. M_2 Surface and internal tides on the Scotian Sheif and slope. J. Mar. Res. 33 (3) 303-323.

Petrie, B.D. and C. Anderson. 1983. Circulation on the Newfoundland Continental Shelf. Atm. Ocean. 207-226.

Phillips, O.M. The Dynamics of the Upper Ocean. 1977. Cambridge Univ. Press. 336. pp.

Raj, P.P.K. and R.A. Griffiths. 1979. The survival of oil slicks on the ocean as a function of sea state limit. 1979 Oil Spill Conference Proceedings. pp. 719-724.

Rallison, J.M. 1984. The deformation of small viscous drops and bubbles in shear flows. Ann. Rev. Fluid Mech. 16:45-66.

Ring Group. 1981. Gulf Stream cold-core rings: their physics, chemistry and biology. Science, 212: 1091-1100.

Simpson, J.H. 1981. The shelf-sea fronts: implications of their existence and behaviour. Phil. Trans. R. Soc. Land. A. 302:531-546.

Simpson, J.H. and R.D. Pingree. 1978. Shallow sea fronts produced by tidal stirring. In: "Oceanic Fronts in Coastal processes". Proc. Edt. by M.J. Bowman and W.E. Esaias. Springer-Verlag. p. 29:42.

Simpson, J.H. and J.R. Hunter. 1974. Fronts in the Irish Sea. Nature Vol. 250: 404-406.

Smith, P.C. 1978. Low-frequency fluxes of momentum, heat, salt and nutrients at the edge of the Scotian shelf. J. Geophys. Res. 83: 4079-4096.

Smith, P.C. 1983. The mean and seasonal circulation off southwest Nova Scotia. J. Phys. Ocean. 13: 1034-1054.

Smith, P.C. and B.D. Petrie. 1982. Low frequency circulation at the edge of the Scotian Shelf. J. Phys. Ocean 12:28-46.

Stommel, H. The Gulf Stream. 1965. Univ. of Calif. Press, Berkely, Calif. 248 pp.

Sutcliffe, W.H., R.H. Loucks and R.F. Drinkwater. 1976. Coastal circulation and physical oceanography of the Scotian Shelf and Gulf of Maine. J. Fish. Res. Bd. Can., 33, 98-115.

Tennekes, H. and J.L. Lumley. A first course in turbulence. 1972. MIT Press, Cambridge, Ma. 300 pp.

Thomson, R. 1981. Oceanography of the British Columbia Coast. Can. Spec. Publ. Fish. Aquat. Sci. 56, 261 pp.

Thorpe, S.A. 1975. The excitation, dissipation and interaction of internal waves in the deep ocean. J. Geophys. Res. 80:328-338.

Thorpe, S.A. 1984(a). A model of the turbulent diffusion of bubbles below the sea surface. J. Phys. Ocean. 14:841-854.

Thorpe, S.A. 1984(b). On the determination of K_v in the near-surface ocean from acoustic measurement of bubbles. J. Phys. Ocean. 14:855-863.

Thorpe, S.A. 1984(c). The effect of Langmuir circulation on the distribution of submerged bubbles caused by breaking wind waves. J. Fluid Mech. 142: 151-170.

Trites, R.W. 1972. The Gulf of St. Lawrence from a pollution viewpoint. In: "Marine Pollution and Sea Life". FAO 1979. p. 59-72.

Trites, R.W. and A. Walton. 1975. A Canadian Coastal Sea - The Gulf of St. Lawrence. Bedford Inst. of Ocean. Report Series BI-R-75-15.

Turner, J.S. 1980. Small-scale mixing processes. In: "Evolution of Physical oceanography - Scientific Surveys in Honor of Henry Strommel". Ed. by B.A. Warren and C. Wunsch. MIT Press. Cambridge. p. 236 - 262.

Vermersh, J.A., R.C. Beardsley and W.S. Brown. 1979. Winter circulation in the western Gulf of Maine. Part 2. Current and pressure observations. J. Phys. Ocean. 9:768-784.

Williams, G.N., R. Hann and W.P. James. 1975. Predicting the fate of oil in the marine environment. Proc. of the Joint Conference on Prevention and Control of Oil Spills. Amer. Pet. Inst. Wash. D.C. pp. 567-572.

Zimmerman, J.T.F. 1978. Dispersion by tide-induced residual current vortices. In "Hydrodynamics of Estuaries and Fjords". Proc. of the 9th Intern. Liege Colloq. on Ocean Hydrodynamics. Ed. by J.C.J. Nihoul, Elsevier. P 207-216.

Zimmerman, J.T.F. 1976. Mixing and flushing of tidal embayments in the Western Dutch Wadden Sea. Part II: Analysis of mixing processes. Neth. J. of Sea Res. 10:399-439.